Black Holes and Wave Mechanics

Sam R. Dolan

February 26, 2008

Abstract

This is a short introductory course on wave mechanics on black hole space-times. Its main focus is on the the classical Klein-Gordon field on the Schwarzschild spacetime. As well as being of interest in its own right, the scalar field serves as a simple 'toy model' which offers insight into the dynamics of gravitational radiation. Later, as an example of a quantum-mechanical field, we consider the Dirac equation.

The course begins with a brief introduction to General Relativity and the Schwarzschild space time. We discuss coordinate singularities, and the relative merits of various coordinate systems. The scalar wave equation is introduced along with its conserved current. Appropriate physical boundary conditions are discussed, and the behaviour of the field at the origin, the horizon and infinity is scrutinised.

We examine the field dynamics by evolving the $1+1$ PDEs in the time domain. We show that bombarding the black hole with Gaussian wavepackets results in the excitation of 'quasi-normal modes' (QNMs). These modes have specific frequencies and decay rates that provide a signature for the underlying black-hole space-time. Two methods for calculating QNMs are discussed.

In the final part of the course, we look at time-independent scattering. We consider a monochromatic, long-lasting planar wave impinging on a black hole. In the long-wavelength regime $\lambda \gg r_s$, a perturbative approach is valid. We show how to expand the scattering amplitude in a Born series, and compute the lowest-order amplitude in two coordinate systems. For higher couplings $\lambda \gtrsim r_s$, a partial wave approach is more appropriate. A range of interesting diffraction effects are seen in the scattered signal.

Preface

These notes were prepared for a short course given at the *First Amazonian School on Quantum Theory* held in Belem in Brazil on 25th - 29th February 2008. The course is for final-year undergraduates and graduate students who may have no background in General Relativity. Very little material in these notes is original. I have drawn from a range of excellent sources, in particular the textbooks by d'Inverno [4], Poisson [16] and MTW [2]. The sections on wave scattering owe much to the review article by Andersson and Jensen [1] and Chapter 4 in Frolov and Novikov [8], and the papers by Leaver [12, 13]. Some material from my thesis [5] is included, which owes a great debt to the work by my supervisors A. Lasenby and C. Doran [10, 6, 11]. A metric signature $\{+---\}$ is used throughout.

Please let me know of any typos or inaccuracies at *sam.dolan@ucd.ie*.

Contents

1 Introduction **3**

2 Basics of General Relativity **4**

2.1 Newtonian and Einsteinian Gravity 4

2.1.1 Special Relativity 5

2.1.2 General Relativity 6

2.2 The Schwarzschild Solution 7

2.3 Alternative Coordinate Systems 11

2.4 Gravitational Lensing 11

3 Waves on the Schwarzschild Space-Time **13**

3.1 The Scalar Field 13

3.1.1 Current 15

3.1.2 Flux through the horizon 16

3.1.3 Alternative coordinate systems 17

3.2 The Dirac Equation* 18

3.2.1 Dirac equation on the Schwarzschild space-time 19

3.2.2 Current 20

3.2.3 Separation of variables 20

3.2.4 Flux conservation 21

3.2.5 Behaviour near the origin 21

4 Time-Dependent Wave Mechanics **22**

4.1 Wavefront scattering 22

4.2 Wavepacket scattering 24

4.3 Quasi-Normal Modes 24

4.4 Green's Function Analysis 28

4.4.1 Contour integration 30

4.5 Bound States 30

4.5.1 Non-relativistic bound state spectrum 32

4.5.2 Continued Fraction Method 33

5 Time Independent Scattering and Absorption **36**

5.1 Perturbative Scattering Theory 37

5.1.1 Klein-Gordon scattering 38

5.1.2 Amplitude in Eddington-Finkelstein coordinates 39

5.1.3 Amplitude in Painlevé-Gullstrand coordinates 40

5.1.4 Spin-half scattering 42

5.2 Partial Wave Analysis 43
5.2.1 The comparison Newtonian problem 44
5.2.2 Partial wave amplitudes 45
5.2.3 Absorption 48

6 Further Topics⋆ 50
6.1 The Dirac Equation 50
6.1.1 Tetrads and the spin-connection 51
6.1.2 Derivative operator for the Dirac field 52
6.1.3 The Dirac equation on a Schwarzschild background 53

1 Introduction

Light cannot escape the lure of a black hole; neither, it seems, can theoretical physicists! Even the *idea* of a black hole – an "invisible" region of space-time harboring an inescapable spacetime-distorting attractor – has its own irresistible force. Poetically speaking, a generation of physicists are bound to the idea. If you wish to escape the pervasive influence of the black hole, put down these notes immediately, and study something sensible instead. If not, read on!

Despite their outlandish nature, black holes are taken very seriously by astrophysicists. A black hole is thought to represent the ultimate outcome of gravitational collapse. For example, it is believed that solar-mass-sized black holes reside in certain binary systems in galaxy. It is suspected that the merger of a pair of black holes may be responsible for the gamma ray bursts sporadically observed by astronomers. There is strong evidence for a supermassive black hole at the centre of our galaxy. Quasars are thought to be due to powerful ejections of energy by supermassive black holes in distant galaxies.

This is exciting stuff for astrophysicists, but you may reasonably ask: what do black holes have to do with quantum theory? Let me suggest three partial answers. Firstly, mathematical techniques developed for wave mechanics (e.g. partial wave series; WKB methods; Born approximation; scattering expansions) may be fruitfully applied to problems in classical gravitational theory. Secondly, black holes are simple examples of generic systems which scatter, absorb and emit radiation. It is hoped that analogue systems with similar properties will soon be created and investigated in the laboratory. Finally, it is anticipated that General Relativity may eventually be unified with quantum theory in a theory of Quantum Gravity. String Theory and Loop Quantum Gravity are modern contenders for this 'holy grail' of physics. Hints on the nature of Quantum Gravity may be obtained by studying the interaction of quantum fields with strongly-gravitating systems, such as black holes.

It is widely felt that gravity is somehow *different* to the other three forces (electromagnetic, weak and strong). In the lab, the interaction of particles are satisfactorily described by the renormalizable quantum field theories that make up the Standard Model. Yet gravity refuses to fit into the Standard Model straightjacket. For an experimental particle physicist, this is rarely a practical problem. Gravity is significantly weaker than the other forces, and may be safely

neglected in the lab. For instance, the electromagnetic force between two electrons is $\approx 10^{40}$ times larger than the corresponding gravitational force! In common experience, the influence of gravity is only significant on the macroscale. Explaining this hierarchy problem (i.e. the apparent relative weakness of gravity) is a major goal of theoretical physics.

Why is gravity so troublesome? Well, General Relativity (GR) – our best-tested and most elegant theory of gravity – is based on the assumption that space-time is intrinsically smooth and continuous on the smallest scales. Yet, quantum theory suggests that on a length scale ΔL there is an uncertainty in the energy of $\Delta E \sim hc/\Delta L$. In turn, GR implies that energy creates space-time curvature. Hence, at tiny distances, $\Delta L \sim l_P$ (where $l_P \sim 1.6 \times 10^{-35}$ m) there is enough energy density in the vacuum to significantly distort space-time. In other words, quantum theory predicts the breakdown of GR on scales smaller than l_P, or energies greater than $M_P \sim 1.22 \times 10^{19}\text{GeV}/c^2$ (estimated by equating the Compton wavelength of a particle, $\lambda = hc/(Mc^2)$, to its Schwarzschild radius $r_s = 2GM/c^2$).

This is not a course in Quantum Gravity! Instead, we will study some simple but relevant problems in gravitation that can be studied using wave-mechanics methods.

2 Basics of General Relativity

2.1 Newtonian and Einsteinian Gravity

In the Newtonian universe, space and time are distinct entities. Time is **universal**. In other words, all observers can agree on the rate of progress of time, regardless of their individual frames of reference. Time marches forward in a steady inviolate fashion, disregarding the particular motion of nearby apples, stars and galaxies. Idealised clocks, once synchronized, remain in perfect agreement for eternity. To describe particle motion in Newtonian physics it is natural to use t – a universal time coordinate – to parameterize the spatial position $x^i = [x, y, z]$. Newton's Laws provide us with differential equations, which we solve to determine the functions $x^i(t)$. In common experience we find the our world to be nearly 'Newtonian'. This is because we generally move about at relative speeds much smaller than the speed of light $c \approx 3 \times 10^8 \text{ms}^{-1}$.

In the Einsteinian view of the universe, time is *not* universal. Two 'events' that appear to occur simultaneously to one observer do not necessarily appear to occur simultaneously to other observers. In the Einstein universe, space and time must be unified into a 4D space-time. Events in a 4D space-time are labelled with four coordinates, for example $x^\mu = [x^0, x^1, x^2, x^3]$. The 0th coordinate is usually thought of as a 'time' coordinate, $x^0 = ct$. But beware, time is observer-dependent concept, and interpretation of x^0 is not always straightforward. Firstly, there is great freedom in our choice of coordinate system; secondly, it is not always possible to describe the whole space-time using a single coordinate system.

A particle moving in space-time describes a **world-line**. A world-line is just a continuous path through coordinate space; this path can be described by a set of four coordinate functions $x^\mu(\lambda) \equiv [x^0(\lambda), x^1(\lambda), x^2(\lambda), x^3(\lambda)]$. The **affine parameter** λ plays the same role in parametrizing motion in a 4D space-time that t played for 3D trajectories. In many situtations the affine

parameter will be chosen to correspond to the *proper time*: the time as measured by an observer moving along the world-line.

In a moment, we will derive differential equations which we can solve to find a given particle world-line. Before that, let us begin by considering motion in flat (i.e. empty, non-gravitating) space-times, described by **Special Relativity**.

2.1.1 Special Relativity

'Special' relativity is limited in validity to Minkowski space-time. Minkowski space-time is globally 'flat', i.e. free from gravitational influences (which are experimentally measurable as tidal forces). In Minkowski space-time there are special set of coordinate charts. Each chart in the set corresponds to a particular **inertial observer**. Intuitively, an inertial observer is one who feels no force, and any pair of inertial observers must be in constant relative motion. The coordinates $x^0 = ct$ and $x^i = [x, y, z]$ in these charts are defined by the times and distances measured by an inertial observer.

Suppose now an inertial observer measures 'coordinate distances' between a pair of space-time events, and finds $\Delta x^0 = c\Delta t$ and Δx^i. A second inertial observer measures the 'coordinate distances' $\Delta x^{0\prime} = c\Delta t'$ and $\Delta x^{i\prime}$. The coordinate distances according to the two observers are related by a **Lorentz transformation**. For example, if the second observer is moving in the $+x$ direction at speed v relative to the first observer, then

$$c\Delta t' = \gamma\left(c\Delta t - v\Delta x/c\right), \qquad \Delta y' = \Delta y \tag{1}$$

$$\Delta x' = \gamma\left(\Delta x - v\Delta t\right), \qquad \Delta z' = \Delta z, \tag{2}$$

where

$$\gamma = \left(1 - v^2/c^2\right)^{-1/2}. \tag{3}$$

Whilst any pair of inertial observers will disagree about coordinate distances and times, there is one quantity on which they both agree: the space-time **interval**. On a flat space-time the interval is

$$(\Delta s)^2 = (c\Delta t)^2 - (\Delta x)^2 - (\Delta y)^2 - (\Delta z)^2. \tag{4}$$

Note that the interval $(\Delta s)^2$ is invariant under Lorentz transformations; all inertial observers will measure the same interval between a given pair of events. The interval $(\Delta s)^2$ may take either sign. The sign of the interval tells us about the causal relationship between the two events. The interval is said to be either:

- **time-like** if $(\Delta s)^2 > 0$,
- **space-like** if $(\Delta s)^2 < 0$, or,
- **null** if $(\Delta s)^2 = 0$.

If the interval between a pair of events is space-like, then there exists an inertial frame in which the two events occur simultaneously. If the interval is time-like, then there exists an inertial

frame in which the two events occur at the same position. If the interval is null, then the two events may be connected by a ray of light.

In classical relativity, light rays (and massless particles) propagate along null world-lines (i.e. paths along which the change in interval is zero). Particles with non-zero mass follow time-like world-lines. The change in interval Δs is proportional to the **proper time** experienced by an observer moving along the world-line, $\Delta\tau = \Delta s/c$.

2.1.2 General Relativity

If the space-time contains gravitating matter, then global definitions such as (4) are inappropriate. In this case, the structure of space-time varies from point to point – 'over there' may be quite different from 'over here'. The space-time interval is still a well-defined concept, but it is expressed in differential form,

$$ds^2 = \sum_{\mu=0}^{3}\sum_{\nu=0}^{3} g_{\mu\nu}(x)dx^\mu dx^\nu. \tag{5}$$

This is known as the **line element**. Here, ds is the infinitessimal space-time interval between the neighbouring events at x^μ and $x^\mu + dx^\mu$. Here, $g_{\mu\nu}(x)$ is a symmetric tensor called the **metric**. Each of its coefficients is a function of space-time position. The metric determines the interval between neighbouring points. Once a metric is specified, it is straightforward to calculate the world-lines of free particles using an action principle.

The interval along a world-line $x^\mu(\lambda)$ is found by integrating along the world-line,

$$\Delta s = \int d\lambda \sqrt{\sum_{\mu=0}^{3}\sum_{\nu=0}^{3} g_{\mu\nu}(x(\lambda))\frac{dx^\mu}{d\lambda}\frac{dx^\nu}{\lambda}}. \tag{6}$$

If the world-line is time-like, then the interval Δs gives the proper time experienced by the particle. If the world-line is null, then $\Delta s = 0$.

From here on, we will adopt a standard **summation convention**: we automatically sum over any pair of indices that appear once 'upstairs' and once 'downstairs'. For example, $a^\mu b_\mu \equiv \sum_{\mu=0}^{3} a^\mu b_\mu$. We will also use 'dot' notation to denote differentiation with respect to λ, i.e. $\dot{x}^\mu \equiv \frac{dx^\mu}{d\lambda}$.

The summation convention is more than a labour-saving device. It reminds us that when taking a sum over two indices, one index must be 'upstairs' and one must be 'downstairs' for the resultant quantity to have physical significance. Why is this? Well, under a general coordinate transformation $x \mapsto x' = x^{\mu\prime}(x^\nu)$, the 'upstairs' and 'downstairs' indices transform in opposite ways:

$$\dot{x}^{\alpha\prime} = \frac{\partial x^{\alpha\prime}}{\partial x^\mu}\dot{x}^\mu, \qquad \dot{x}_{\alpha\prime} = \frac{\partial x^\mu}{\partial x^{\alpha\prime}}\dot{x}_\mu. \tag{7}$$

The upper indices transform like the infinitessimal coordinate distances dx^μ; the lower indices transform like coordinate derivatives (i.e. by the chain rule, $\frac{\partial}{\partial x^{\alpha\prime}} = \frac{\partial x^\mu}{\partial x^{\alpha\prime}}\frac{\partial}{\partial x^\mu}$). Only by summing over upper and lower indices we can recover a scalar quantity that is independent of coordinate frame.

Indices are lowered and raised using the metric $g_{\mu\nu}$ and metric inverse $g^{\mu\nu}$,

$$\dot{x}_\mu = g_{\mu\nu}\dot{x}^\nu, \qquad \dot{x}^\mu = g^{\mu\nu}\dot{x}_\nu. \tag{8}$$

The metric inverse is defined by the identity

$$g^{\mu\nu}g_{\nu\lambda} = \delta^\mu_\lambda. \tag{9}$$

How do we find the world-lines of free particles? The answer is simple: *free particles follow* ***geodesics*** *in curved space.* A **geodesic** is the relativistic generalisation of the idea of a straight line. In a Euclidean geometry, a straight line is the shortest line that joins two points. In curved space-time, a geodesic is the path between two points along which the interval is extremal. Hence, geodesics are found by extremising an action S which is just the space-time interval.

Let us now put this statement in mathematical form. Using this notation, the action for a free-particle is

$$S \equiv \Delta s = \int L(x^\mu(\lambda), \dot{x}^\mu(\lambda))d\lambda \tag{10}$$

where

$$L(x^\mu(\lambda), \dot{x}^\mu(\lambda)) = [g_{\mu\nu}(x)\dot{x}^\mu\dot{x}^\nu]^{1/2} \tag{11}$$

The equations of motion are found from the Euler-Lagrange equations,

$$\frac{\partial L}{\partial x^\mu} - \frac{d}{d\lambda}\left(\frac{\partial L}{\partial \dot{x}^\mu}\right) = 0. \tag{12}$$

2.2 The Schwarzschild Solution

The first exact solution of Einstein's field equations was found by Karl Schwarzschild [18] during the First World War. The Schwarzschild solution describes the geometry of space-time exterior to a non-rotating spherical gravitational source in vacuum. To a good approximation, the Schwarzschild solution describes the field of a star such as our sun. The solution has only one free parameter, the gravitational mass M. The Schwarzschild solution is the only possible asymptotically-flat solution allowed by the constraint of spherical symmetry. This implies that the space-time outside an isolated spherical source is unchanging, regardless of any internal radial motions.

The Schwarzschild spacetime is usually described with the coordinates $\{t, r, \theta, \phi\}$ and the line element

$$ds^2 = (1 - 2M/r)dt^2 - (1 - 2M/r)^{-1}dr^2 - r^2(d\theta^2 + \sin^2\theta d\phi^2). \tag{13}$$

(Interestingly, this is *not* the form in which Schwarzschild originally presented his solution. We shall see in a moment that there are many other choices of coordinates). Here, we are using units in which $G = c = 1$. Whenever we put units back in, we should remember that M represents the length $M \equiv GM/c^2$.

A source lying entirely within its gravitational horizon at $r_h = 2GM/c^2$ is known as a "Schwarzschild black hole". The prospect of such dense objects having physical reality was first

raised by studies of gravitational collapse and white dwarf stability in the 1930s. However, such solutions were only studied in detail from the 1960s onwards; the term "black hole" was coined in 1968 by John Wheeler.

Let's examine the geodesics of the Schwarzschild space-time. To do so, we insert the line element (13) into the Lagrangian (11) and find the Euler-Lagrange equations. Without loss of generality, let us restrict our attention to the equatorial plane $\theta = \pi/2$. Since the metric is independent of t and ϕ, the corresponding E-L equations lead to two constants of motion

$$k = (1 - 2M/r)\dot{t}, \tag{14}$$

$$h = r^2\dot{\phi}. \tag{15}$$

It is natural to call k the 'energy' and h the 'angular momentum' of the geodesic.

To find an equation for the radial coordinates, $\dot{r}$, we could write down the corresponding Euler-Lagrange equation. But actually, it is simpler to use the line element (13) directly. If the geodesic is null, then $ds^2 = 0$. If the geodesic is time-like then we can choose the affine parameter λ to be equal to the proper time τ. Then we can rewrite (13) as

$$(1 - 2M/r)\dot{t}^2 - (1 - 2M/r)^{-1}\dot{r}^2 - r^2\dot{\phi}^2 = \epsilon^2, \qquad \text{where} \quad \epsilon^2 = \begin{cases} 0 & \text{null} \\ 1 & \text{time-like} \end{cases} \tag{16}$$

Substituting the constants of motion k and h into 16 yields an *energy equation* for the radial coordinate,

$$\tfrac{1}{2}\dot{r}^2 + V_{\text{eff}}(r) = \frac{k^2 - \epsilon^2}{2}, \tag{17}$$

with an effective potential

$$V_{\text{eff}}(r) = -\frac{M\epsilon^2}{r} + \frac{h^2}{2r^2} - \frac{Mh^2}{r^3}. \tag{18}$$

The effective potential is plotted in Fig. 1 for various timelike geodesics.

It is interesting to compare the Schwarzschild effective potential with the Newtonian effective potential, $V_{\text{eff}}^{\text{Newt.}} = -M/r + h^2/2r^2$. Both are attractive in the far-field, and both have an angular momentum potential barrier. However, in the Schwarzschild case, the barrier disappears as the horizon is approached: $V_{\text{eff}} \to -\infty$ as $r \to 2M$. In other words, large angular momentum is not sufficient to prevent a geodesic from spiralling in to a black hole.

A local minimum in the potential corresponds to a stable circular orbit with $\dot{r} = 0$. A local maximum corresponds to an *unstable* circular orbit – a feature which is not present in the Newtonian case.

Exercise:

- Show that the unstable photon (i.e. null) orbit is at $r = 3M$.
- Show that the stable time-like orbit is at $r = (h^2/2M)\left(1 + \sqrt{1 - 12M^2/h^2}\right)$.
- Show that the innermost stable time-like orbit is at $r = 6M$.

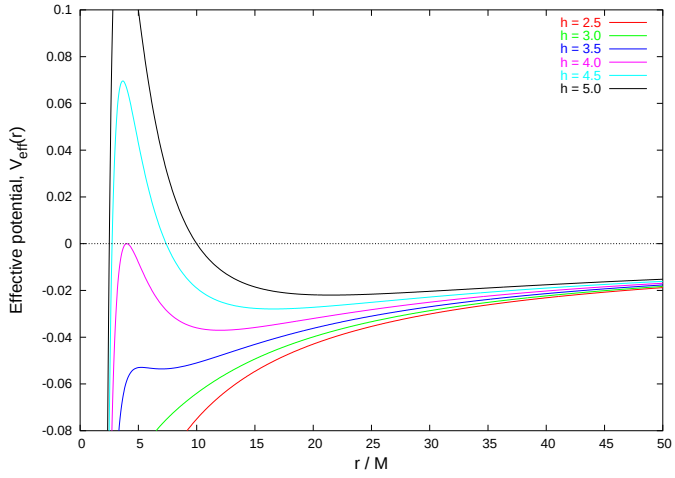

Figure 1: *Classical effective potential.* This plot shows the effective potential for timelike geodesics with a range of angular momenta $h = r^2\dot{\phi}$.

Let us consider geodesics approaching from infinity, such as those shown in Fig. 2. If their energy $(k^2 - \epsilon^2)/2$ is higher than the peak of the potential barrier then they will be absorbed by the black hole. As is clear from Fig. 2, trajectories that make too close an approach to the hole spiral inwards, and end on the singularity. The last geodesic to avoid the singularity defines a critical impact parameter b_c. All geodesics with $b > b_c$ are scattered, whereas all geodesics with $b < b_c$ are absorbed.

The value of b_c may be found by considering the height of the peak of the effective potential barrier. It is found to be

$$b_c = \frac{M}{\sqrt{2}v^2}\left(8v^4 + 20v^2 - 1 + (1+8v^2)^{3/2}\right)^{1/2}. \tag{19}$$

where v is the particle speed at infinity $v = \sqrt{k^2 - \epsilon^2}/k$, and b is the impact parameter $b = h/vk$. The classical absorption cross section σ_a is just the area of the circle defined by the critical impact parameter, $\sigma_a = \pi {b_c}^2$.

Exercise: show that, for null geodesics, the critical impact parameter is simply $b_c = 3\sqrt{3}M$.

A shortcoming of the Schwarzschild coordinate system is that it takes an infinite coordinate time t for ingoing geodesics to reach the horizon. Let us examine this statement more carefully. Consider a radially-ingoing time-like geodesic for which $\epsilon^2 = 1$ and $h = 0$. Let us make the choice $k = 1$, which corresponds to dropping in a particle from infinity with zero initial speed. Then (17) implies $\dot{r}^2 = 2M/r$. By taking the negative square root and integrating we find

$$\tau - \tau_0 = \frac{2}{3(2M)^{1/2}}\left(r_0^{3/2} - r^{3/2}\right) \tag{20}$$

where the particle is at r_0 at proper time. Rather surprisingly, this is exactly the same as the Newtonian result (but with proper time τ in place of t). No singular behaviour occurs at the Schwarzschild radius and the body falls continuously to $r = 0$ in a finite proper time.

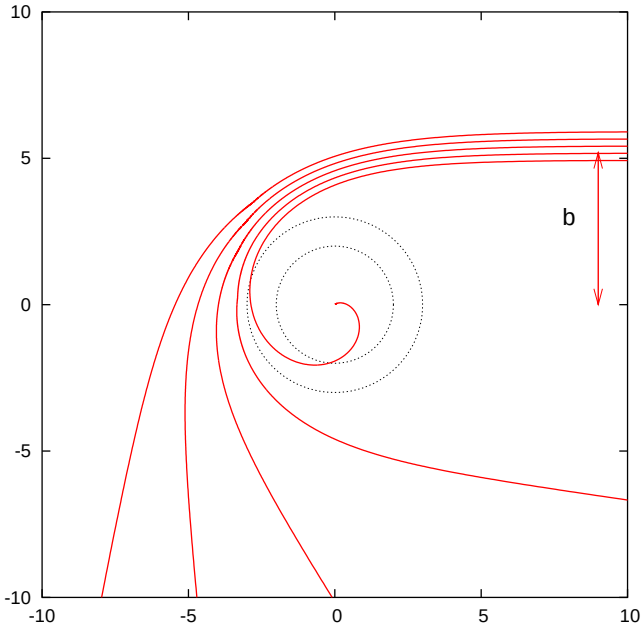

Figure 2: *Photon geodesics around a Schwarzschild black hole.* The plot shows trajectories close to the critical impact parameter $b_c = 3\sqrt{3}M \approx 5.196M$. The inner circle shows the event horizon at $r = 2M$, and the outer circle shows the unstable photon orbit at $r = 3M$.

However, if we attempt to describe the same motion in terms of the coordinate time t then

$$\frac{dt}{dr} = \frac{\dot{t}}{\dot{r}} = -\left(\frac{r}{2M}\right)^{1/2}\left(1 - \frac{2M}{r}\right) \tag{21}$$

This expression is infinite at $r = 2M$. The coordinate time t diverges logarithmically as the horizon is approached.

Exercise:

- Show that

$$t - t_0 = -\frac{2}{3(2M)^{1/2}}\left(r^{3/2} - r_0^{3/2} + 6Mr^{1/2} - 6Mr_0^{1/2}\right) + 2M \ln \frac{(\sqrt{r} + \sqrt{2M})(\sqrt{r_0} - \sqrt{2M})}{(\sqrt{r_0} + \sqrt{2M}(\sqrt{r} - \sqrt{2M}))}. \tag{22}$$

- Assume a photon is emitted radially by a observer fixed at the point $r = r_0$, and detected by an observer fixed at $r = r_1$. Show that its frequency is redshifted by $1 + z = \omega_1/\omega_0 = \sqrt{(1 - 2M/r_1)/(1 - 2M/r_0)}$. (*Hint:* the observed frequency is proportional to $\dot{x}^\mu k_\mu$, where $\dot{x}^\mu$ is the world-line of the observer, and k^μ is the null geodesic followed by the photon.)

In summary, a geodesic reaches the horizon in a finite proper time, but takes an infinite coordinate time t. Proper time is a physical quantity that has a clear, observer-independent meaning – it is the time measured by an infalling observer. The divergence at $r = 2M$ is just a *coordinate singularity*. The Schwarzschild coordinate time t is not well-defined at $r = 2M$. In contrast, at $r = 0$ there is a physical singularity: here, space-time curvature (and thus the physically-measurable tidal force) is infinite.

2.3 Alternative Coordinate Systems

The coordinate singularity can be removed by breaking the time-symmetry implicit in the diagonal form of the metric. If we define a new time coordinate $\bar{t}$ by

$$\bar{t} = t + 2M\ln(r-2M) \qquad \Rightarrow \qquad d\bar{t} = dt + \frac{2M}{r-2M}dr \tag{23}$$

then the line element (13) becomes

$$ds^2 = (1-2M/r)d\bar{t}^2 - (4M/r)dr d\bar{t} - (1+2M/r)dr^2 - r^2(d\theta^2 + \sin^2\theta d\phi^2). \tag{24}$$

This is the Schwarzschild solution in **Advanced Eddington-Finkelstein** (AEF) coordinates. It is well-suited to describing ingoing null geodesics.

Alternatively, one can define a new time coordinate $\tilde{t}$ by

$$\tilde{t} = t + 4M\left(\sqrt{r/2M} + \frac{1}{2}\ln\left|\frac{\sqrt{r/2M}-1}{\sqrt{r/2M}+1}\right|\right) \qquad \Rightarrow \qquad d\tilde{t} = dt + \frac{\sqrt{2Mr}}{r-2M}dr \tag{25}$$

which leads to the Schwarzschild solution in **Painlevé-Gullstrand** coordinates,

$$ds^2 = (1-2M/r)d\tilde{t}^2 - \sqrt{\frac{8M}{r}}dr d\tilde{t} - dr^2 - r^2(d\theta^2 + \sin^2\theta d\phi^2) \tag{26}$$

The time coordinate $\tilde{t}$ has a natural interpretation: it is the proper time as measured by a radially infalling observed who starts from rest at infinity. A further advantage is that hypersurfaces of constant $\tilde{t}$ are spatially flat.

Exercise:

- Show that radially-ingoing null geodesics are given by $\dot{r} = -\dot{\tilde{t}}$ in this system.
- Show that in Painlevé-Gullstrand coordinates, an radially-infalling path with $k = 1$ is described by
$$\dot{r} = -\sqrt{\frac{2M}{r}}, \qquad \dot{t} = 1. \tag{27}$$
- **Isotropic Coordinates**. Define a new radial coordinate ρ by $r = \rho + m + m^2/4\rho$. Show that the metric becomes
$$ds^2 = \frac{(1-M/2\rho)^2}{(1+M/2\rho)^2}dt^2 - (1+M/2\rho)^4\left(d\rho^2 + \rho^2 d\theta^2 + \rho^2\sin^2\theta d\phi^2\right). \tag{28}$$

2.4 Gravitational Lensing

Light is deflected by a gravitational field. Or rather, light follows a locally 'straight line' (a null geodesic) in a curved space-time. In 1919, a team of astronomers led by Eddington measured the angle of deflection of starlight during a solar eclipse. As an application of the techniques of the previous section, let us derive the so-called "Einstein deflection angle" that was measured.

Dividing the "energy equation" (17) by the square of the angular velocity, $\dot{\phi} = h/r^2$ leads to the *orbit equation*,

$$\left(\frac{du}{d\phi}\right)^2 + u^2 = \frac{k^2 - \epsilon^2}{h^2} + \frac{2M\epsilon^2}{h^2}u + 2Mu^3 \tag{29}$$

where $u = 1/r$. Differentiating, we obtain the general-relativistic version of Binet's equation,

$$\frac{d^2u}{d\phi^2} + u = \frac{M\epsilon}{h^2} + 3Mu^2. \tag{30}$$

It differs from the Newtonian equivalent through the presence of the last term.

For a light ray, $\epsilon^2 = 0$. In the absence of a gravitating body (i.e. $M = 0$), Binet's equation has a very simple solution:

$$u_0(\phi) = \frac{1}{b}\sin(\phi) \tag{31}$$

This is a straight line, with ϕ going from 0 to π, and $u = 1/r$ going from 0 to $1/b$ and back again. Here, b is the distance of closest approach – the **impact parameter**.

In the weak-field (i.e. far from the horizon, $r \gg 2M$) Binet's equation can be solved perturbatively, by expanding the solution in powers of M/b ,

$$u \approx u_0 + (M/b)u_1 + \mathcal{O}(M^2/b^2) \tag{32}$$

so that

$$\frac{d^2u_1}{d\phi^2} + u_1 = 3b{u_0}^2 = 9\sin^2(\phi)/b. \tag{33}$$

This has the solution $u_1 = 3(1+C\cos\phi+\cos^2\phi)/b$ (exercise). Let us assume the two asymptotes of the trajectory are $\phi = -\delta_1$ and $\phi = \pi + \delta_2$. We can find the angle of deflection by setting $u_0 + (M/b)u_1 = 0$ and using small-angle approximations to get

$$-\frac{\delta_1}{b} + \frac{M}{b^2}(2 + C) = 0, \tag{34}$$

$$-\frac{\delta_2}{b} + \frac{M}{b^2}(2 - C) = 0, \tag{35}$$

$$\Rightarrow \Delta\phi = \delta_1 + \delta_2 = 4M/b \tag{36}$$

The Einstein deflection angle is twice the Newtonian deflection angle. In certain astrophysical situations, a massive body can act light a gravitational lens, focussing parallel rays from a distant source. The first observation of this phenomenon came in 1979, when astronomers discovered that the light seemingly from two point sources separated by 6 seconds of arc (1/600 degree) actually originated from a single quasar.

There are a range of other experimental tests of GR, including the advance of the perehelion of Mercury; gravitational redshift and time dilation; and tests of the equivalence principle (e.g. the Eötvös experiment). One of the most exciting contemporary experiments is Gravity Probe B, which is seeking to measure the frame-dragging effect caused by the rotation of the Earth. It is due to report results later in 2008.

3 Waves on the Schwarzschild Space-Time

Having briefly considered the scattering of light in the 'geometrical optics' limit, we now look at possible diffraction effects which may arise from wave propagation near black holes. As we will see, the extreme nature of black holes can lead to a variety of interesting effects. To understand these effects we develop a framework for studying the scattering of waves by black holes.

From an observational point of view, the most interesting cases for study are electromagnetic and gravitational waves. Gravitational waves (GWs) are a key prediction of GR, but have yet to be detected directly. This is perhaps not surprising as the expected amplitude of waves reaching Earth is incredibly tiny (with a dimensionless strain of $h \sim 10^{-21}$). There is strong indirect evidence for GWs from pulsar timing observations. There is presently much interest in gravitational waves, since it is hoped a new generation of ground-based gravitational-wave detectors (laser interferometers LIGO, VIRGO, GEO-600) are poised to make a 'first-light' detection. Prospects for the future are good, with a space-based observatory (LISA) planned in the next decade.

Electromagnetic waves are strongly coupled to charged matter. Hence light that passes close to a black hole is unlikely to escape to infinity without undergoing secondary (i.e. non-gravitational) scattering, unless the hole is extremely quiescent and isolated from charged matter. On the other hand, gravitational waves are weakly coupled, and couple only to the bulk motions of large amounts of matter. Their frequencies are directly related to the motion of matter (for example, orbital frequencies). Hence, GWs may offer the best observational window on the near-horizon region of a black hole. Unlike the other fields, the gravitational field is inherently non-linear; however, a linearized approximation works well in many circumstances. Furthermore, the dynamics of the gravitational field can be understood by studying the massless scalar field (for which the mathematics is much simpler!). That is the approach we take here.

Another intriguing physical possibility is the interaction of neutrino waves with black holes. Since neutrinos are uncharged and only interact through the weak force and gravity, the neutrino field may also bear the direct imprint near-horizon physics. Neutrinos have been detected at a number of facilities around the world, but the observed fluxes are currently too low for effective 'neutrino astronomy'. That may change in future decades however.

The fields may be classified by their spin: $s = 1/2$ for neutrinos, $s = 1$ for EM waves, and $s = 2$ for gravitational fields. The latter two fields are massless, and the mass of the neutrino is thought to be non-zero but very small $m_\nu < 1$ meV. Obviously, field equations depend on the spin, and polarization effects induced by spin can be important. However, much of the physics does not depend on spin. In this section we will study the massless scalar ($s = 0$) field for its mathematical simplicity, and the Dirac ($s = 1/2$) field as an example of a wave with spin.

3.1 The Scalar Field

The evolution of a scalar field Φ may be determined from an action principle. Let us assume the field is real, and implicitly take the real part of expressions wherever necessary. The minimally-

coupled action is

$$S = \int d^4x\, \mathcal{L}(\Phi, \partial_\mu \Phi; g_{\mu\nu}) \qquad \text{where } \mathcal{L} = \tfrac{1}{2}\sqrt{-g}\left(g^{\mu\nu}\partial_\mu\Phi\partial_\nu\Phi - \mu^2\Phi^2\right) \tag{37}$$

where partial differentiation is denoted by $\partial_\mu \Phi = \frac{\partial \Phi}{\partial x^\mu}$ and summation convention is assumed. In this expression, g is the determinant of the metric tensor, and μ is the rest mass of the field. We extremise the action by employing the Euler-Lagrange equation

$$\frac{\partial \mathcal{L}}{\partial \Phi} = \frac{d}{dx^\mu}\left(\frac{\partial \mathcal{L}}{\partial(\partial_\mu \Phi)}\right). \tag{38}$$

This leads to the wave equation

$$\frac{1}{\sqrt{-g}}\frac{\partial}{\partial x^\nu}\left(\sqrt{-g}\, g^{\mu\nu}\frac{\partial \Phi}{\partial x^\nu}\right) + \mu^2\Phi = 0. \tag{39}$$

The wave equation is linear, so the total solution may be expressed as a sum over partial waves. The spherical symmetry of the Schwarzschild spacetime allows a decomposition into Fourier modes,

$$\Phi_{lm}(t, r, \theta, \phi) = \frac{u_l(r)}{r} Y_{lm}(\theta, \phi) e^{-i\omega t}, \tag{40}$$

where Y_{lm} are spherical harmonics. This leads to a radial equation

$$\left(1 - \frac{2M}{r}\right)\frac{d}{dr}\left[\left(1 - \frac{2M}{r}\right)\frac{du_l}{dr}\right] + \left[\omega^2 - V_l(r)\right] u_l = 0, \tag{41}$$

with the effective potential

$$V_l(r) = \left(1 - \frac{2M}{r}\right)\left(\frac{l(l+1)}{r^2} + \frac{2M}{r^3} + \mu^2\right). \tag{42}$$

The effective potential for the scalar wave is similar in form to the potential for geodesics (18). The radial equation can be written more succinctly if we define a "tortoise coordinate" r_* by

$$\frac{dr^*}{dr} = \frac{r}{r - 2M} \tag{43}$$

which integrates to

$$r^* = r + 2M \ln\left(\frac{r}{2M} - 1\right). \tag{44}$$

Note that the tortoise coordinate has the effect of pushing the horizon away to $r_* = -\infty$. In some sense, the tortoise coordinate reflects the fact that geodesics take an infinite coordinate time to reach the horizon.

The effect of the black hole on the scalar field may be understood by examining the form of the potential barrier. Fig. 3 shows the potential as a function of r_*, for massless (a) and massive (b) waves. It is clear that the potential barrier has, at most, a single peak. Waves with an energy close to this peak will be partially transmitted and partially reflected; waves substantially below the peak will be mostly reflected, and waves substantially above will be mostly absorbed. In addition, if the wave has mass (Fig. 3b), then the potential may contain

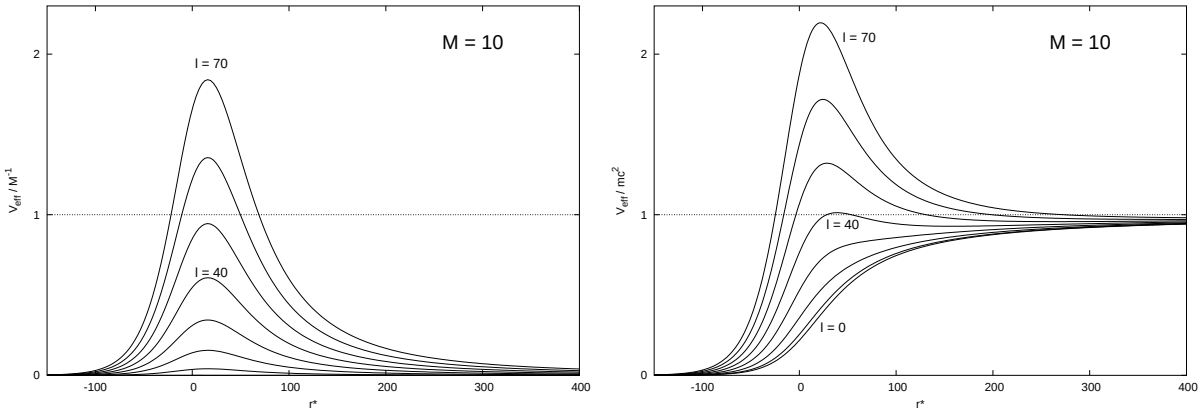

Figure 3: *The effective potential for the scalar field on a Schwarzschild space-time.* (a) For the massless field. The potential is in units of $10\hbar c^3/GM$. (b) For the massive field. The potential is in units of μc^2, where μ is the particle mass, chosen so that $GM\mu/\hbar c = 10$.

a local minimum. This raises the possibility that transient gravitationally-bound states may be induced in this potential well.

The potential tends to constant limits at infinity and the horizon ($r_* \to \pm\infty$). It follows that there are two independent solutions at each of these limits

$$u_l(r) \sim \begin{cases} \exp(\pm i\omega r_*), & r_* \to -\infty, \\ \exp(\pm ipr_*), & r_* \to +\infty, \end{cases} \tag{45}$$

where $p = (\omega^2 - \mu^2)^{1/2}$.

3.1.1 Current

A conservation law can be derived by constructing

$$\Phi^* g^{\mu\nu}\Phi_{;\mu\nu} - \Phi g^{\mu\nu}\Phi^*_{;\mu\nu} = 0. \tag{46}$$

Here, the ; denotes covariant differentiation. The left-hand side is equal to zero by the wave equation, $\Phi^{;\mu}{}_{\mu} = -\mu^2\Phi$. The above expression can be rearranged to

$$J^{\mu}{}_{;\mu} = (-g)^{-1/2}\partial_\mu\left[(-g)^{1/2}g^{\mu\nu}J_\nu\right] = 0, \tag{47}$$

where

$$J_\nu = -\frac{1}{2i}\left(\Phi^*\partial_\nu\Phi - \Phi\partial_\nu\Phi^*\right). \tag{48}$$

J_ν may be interpreted as the conserved four-current of the field.

To find the probability density as perceived by a specific observer, we take the contraction of J_μ and the observer's world line $\dot{x}^\mu$. That is,

$$\rho c^2 = \dot{x}^\mu J_\mu \tag{49}$$

For instance, if we choose an observer at fixed r, θ, ϕ with a world-line vector $\dot{x}^\mu = [(1 - 2m/r)^{-1/2}, 0, 0, 0]$ we find a probability density of

$$\rho c^2 = (1 - 2M/r)^{-1/2}\omega, \tag{50}$$

assuming ω is real. This probability density inevitably diverges at the horizon, since no observer may remain at fixed r for $r \leq 2M$. On the other hand, we may choose a time-like observer falling radially who started from rest at infinity. [***Exercise***: show that this observer has a world-line vector $\dot{x}^\mu = [(1 - 2M/r)^{-1}, -\sqrt{2M/r}, 0, 0]]$. We would expect this observer to measure a well-defined probability density as the horizon was approached. Substituting in the asymptotic form of the radial solution (45) as $r_* \to \infty$,

$$\rho c^2 \sim (1 - 2M/r)^{-1}\omega \left(1 \pm \sqrt{\frac{2M}{r}}\right) \tag{51}$$

$$\sim \omega \left(1 \mp \sqrt{2M}r\right)^{-1} \tag{52}$$

The $\exp(-i\omega r_*)$ solution leads to a probability density that is well-defined at the horzion, but the $\exp(+i\omega r_*)$ solution leads to a divergent probability density. It is natural to infer that only the $\exp(-i\omega r_*)$ solution is physical.

3.1.2 Flux through the horizon

There is a 4D version of Gauss's law that allows us to consider the flux through the horizon. Mathematically stated,

$$\int_V dx^4\sqrt{-g}\, J^\mu{}_{;\mu} = \int_{\partial V} dx^3\sqrt{-h}\, J^\mu \hat{n}_\mu. \tag{53}$$

Here, V is a four-volume with a 3-surface boundary ∂V, $\hat{n}$ is the unit normal to an element of ∂V (assuming not null), and h is the determinant of the induced metric $h_{\mu\nu} = g_{\mu\nu} - \hat{n}_\mu\hat{n}_\nu$.

Let us construct a 'thin-sandwich' four-volume bounded by the four surfaces $t = t_1$, $t = t_1 + dt$, $r = r_0$ and $r = r_1$. The conservation of flux (47) means the left-hand side of (53) is zero, and we can write down a conservation law for the flux in integral form. With a bit of care, one can show

$$\frac{\partial}{\partial t}\left[\int d\Omega \int_{r_0}^{r_1} dr\, r^2 \left(1 - 2M/r\right)^{-1} J_t\right] = -\int d\Omega \left[r^2(1 - 2M/r)J_r\right]_{r_0}^{r_1} \tag{54}$$

Clearly the probability density integral diverges as the horizon is approached. The expression looks simpler if we write in terms of the tortoise coordinate,

$$\frac{\partial}{\partial t}\left(\int d\Omega \int_{r_0}^{r_1} dr_* r^2 J_t\right) = -\int d\Omega \left[r^2 J_{r_*}\right]_{r_0}^{r_1}, \tag{55}$$

but this can't hide the fact that there is a divergence in the left-hand side, due to the coordinate singularity at $r = 2M$.

The same conclusions can be reached by just examining the Wronskian of the radial equation, defined by

$$W = u_1^\dagger \frac{du_2}{dr_*} - u_2^\dagger \frac{du_1}{dr_*}. \tag{56}$$

where † indicates complex conjugation. If ω is real then the radial equation (41) has a conserved Wronskian, and thus $r^2 J_{r_*}$ is constant. In this case, the current flowing through the horizon is exactly matched by the flux incident from infinity. However, there is another possibility that is more natural. If the flux flowing across the horizon is not matched by the flux incident from infinity then ω has an imaginary part, and the Wronskian is *not* conserved.

3.1.3 Alternative coordinate systems

As we have seen, the scalar field oscillates an infinite number of times in approaching the horizon, even though the flux observed by an infalling observer may be well-defined and finite. This is due to the coordinate singularity in the Schwarzschild time at $r = 2M$.

Earlier, we introduced two alternative coordinate systems which penetrate the horizon: advanced Eddington-Finkelstein (AEF) and Painleve-Gullstrand coordinates (PG). Both systems are related to Schwarzschild system by a transformation of the time coordinate

$$t = \bar{t} + \alpha(r), \tag{57}$$

where $\alpha(r)$ is a function of r only which is regular everywhere except at the horizon.

The transformed radial solution $\tilde{u}_l$ is related to the original Schwarzschild field u_l by

$$\tilde{u}_l(r) = e^{-i\omega\alpha(r)} u_l(r). \tag{58}$$

It was noted that geodesics pass through the horizon in a finite coordinate time in the AEF and PG systems. Correspondingly, we would expect to find a scalar wave solution that is well-defined at the horizon in these systems. This is indeed the case, since

$$\alpha_{(\mathrm{AEF})} \sim \alpha_{(\mathrm{PG})} \sim -r_* \sim -2M \ln(r/2M - 1) \qquad \text{as } r \to 2M \tag{59}$$

so the ingoing wave approaches a constant value at the horizon (i.e. it is regular). The outgoing wave on the other hand oscillates as $e^{2i\omega r_*}$ as the horizon is approached, and is not defined at $r = 2M$.

It is relatively straightforward to derive wave equations for the AEF or PG fields, and to examine their properties at $r = 2M$ and $r = 0$.

Exercise:

- By assuming a separation of variables of the form (40), show that the wave equation in AEF coordinates can be written

$$-(r-2M)\frac{\partial^2 R}{\partial r^2} + \left[4iM\omega - \frac{2(r-M)}{r}\right]\frac{\partial R}{\partial r} + \left(\frac{2iM\omega + l(l+1)}{r} - (r+2M)\omega^2 + \mu^2\right) R = 0, \tag{60}$$

  where $R(r) = r u_l$.

- Show that the horizon $r = 2M$ is a regular singular point of the radial equations. By applying the method of Frobenius, show that at the horizon there are two independent solutions which can be written

$$R_{(1)} \sim \sum_{k=0}^{\infty} a_k (r-2M)^k \qquad \text{and} \qquad R_{(2)} \sim (r-2M)^{4iM\omega} \sum_{k=0}^{\infty} b_k (r-2M)^k. \tag{61}$$

- Consider the singular point at the origin $r = 0$. Using the method of Frobenius, derive an indicial equation and show that it has a repeated root $k = 0$. This means there is one regular solution and one that diverges logarithmically:

$$R_{(1)} \sim \sum_{k=0}^{\infty} a_k r^k, \qquad \text{and} \qquad R_{(2)} \sim \ln(r) \sum_{k=0}^{\infty} a_k r^k + \sum_{k=1}^{\infty} b_k r^k \tag{62}$$

  Determine a_1 and b_1 in terms of a_0.

- If the general solution close to the origin is $R \sim A_1 R_{(1)} + A_2 R_{(2)}$, show that to lowest order in r the radial current is

$$J_r = \frac{1}{r} \mathrm{Im}(A_1^* A_2) \tag{63}$$

  Hence show the total flux passing through a sphere around the singularity

$$r^2 \int d\Omega J^r \tag{64}$$

  is well-defined and finite as $r \to 0$.

3.2 The Dirac Equation*

In this section we consider the Dirac equation on the Schwarzschild space-time. The Dirac equation determines the evolution of spin-half matter fields. Its properties are outlined with little justification, and a more detailed exposition is given in Sec. 6.1. A key result is that the Dirac equation takes a particularly simple form when expressed in the Painlevé-Gullstrand coordinate system [11].

In Minkowski space, the free Dirac equation is simply

$$i\hat{\gamma}^\mu \partial_\mu \psi = \mu \psi. \tag{65}$$

where ψ is a four-component *spinor* and $\hat{\gamma}^\mu$ are constant 4×4 matrices satisfying the anti-commutation relations

$$\{\hat{\gamma}^\mu, \hat{\gamma}^\nu\} \equiv \hat{\gamma}^\mu \hat{\gamma}^\nu + \hat{\gamma}^\nu \hat{\gamma}^\mu = 2\eta^{\mu\nu}. \tag{66}$$

There is some freedom in the matrix representation of $\gamma^{'mu}$, but a standard choice is the Dirac-Pauli representation,

$$\hat{\gamma}^0 = \begin{pmatrix} I_2 & 0 \\ 0 & I_2 \end{pmatrix}, \qquad \hat{\gamma}^i = \begin{pmatrix} 0 & \sigma_i \\ -\sigma_i & 0 \end{pmatrix}. \tag{67}$$

Here, I_2 is the 2×2 identity matrix, and σ_i are the Pauli matrices,

$$\sigma_1 = \begin{pmatrix} 0 & 1 \\ 1 & 0 \end{pmatrix}, \qquad \sigma_2 = \begin{pmatrix} 0 & -i \\ i & 0 \end{pmatrix}, \quad \text{and} \quad \sigma_3 = \begin{pmatrix} 1 & 0 \\ 0 & -1 \end{pmatrix}. \tag{68}$$

Using the wave equation we can define a conserved current,

$$J^{\mu}{}_{;\mu} = 0, \qquad \text{where} \qquad J^{\mu} = \psi^{\dagger}\hat{\gamma}^0\hat{\gamma}^{\mu}\psi. \tag{69}$$

where $\psi^{\dagger}$ is the Hermitian conjugate of ψ. [***Exercise***: Derive this result with the aid of the identity $\hat{\gamma}^{\mu\dagger} = \hat{\gamma}^0\hat{\gamma}^{\mu}\hat{\gamma}^0$].

3.2.1 Dirac equation on the Schwarzschild space-time

The Dirac equation on a general curved background can be written as

$$ig^{\mu}\hat{D}_{\mu}\psi = \mu\psi, \tag{70}$$

In this expression, g^{μ} are matrices $g^{\mu} = \hat{\gamma}^a e_a{}^{\mu}$ that satisfy

$$\{g^{\mu}, g^{\nu}\} \equiv g^{\mu}g^{\nu} + g^{\nu}g^{\mu} = 2e_a{}^{\mu}e_b{}^{\nu}\eta^{ab} = 2g^{\mu\nu}. \tag{71}$$

and $e_a{}^{\mu}$ is a local tetrad basis (see Sec. 6.1). The derivative operator is defined by

$$\hat{D}_{\mu} = \partial_{\mu} + \hat{\Omega}_{\mu}, \qquad \text{where } \hat{\Omega}_{\mu} = \frac{i}{2}\omega_{\mu ab}\hat{\Sigma}^{ab}. \tag{72}$$

Note that $\hat{D}_{\mu}$ is matrix-valued. Here, $\omega_{\mu bc}$ is known as the spin-connection, and $\hat{\Sigma}^{ab} = \frac{i}{4}\left[\hat{\gamma}^a, \hat{\gamma}^b\right]$. Full details are outlined in Sec. 6.1.

The Dirac equation turns out to be particularly simple when written in the Painlevé-Gullstrand coordinate system. As we saw earlier, the Painlevé-Gullstrand coordinate system has two distinct advantages: hypersurfaces at constant t are spatially flat; and the PG time coordinate is equivalent to the proper time measured by a free-falling observer, starting from rest. To recover the PG metric, we use the basis

$$g^t = \hat{\gamma}^0, \qquad g^r = \hat{\gamma}^r - \sqrt{\frac{2M}{r}}\,\gamma^0, \qquad \text{where} \quad \hat{\gamma}^r = \frac{1}{r}\sum_i x^i\gamma^i. \tag{73}$$

In the PG system, the Dirac equation may be written in as

$$i\hat{\gamma}^{\mu}\partial_{\mu}\psi + -i\hat{\gamma}^0\sqrt{\frac{2M}{r}}\left(\frac{\partial}{\partial r} + \frac{3}{4r}\right)\psi = \mu\psi, \tag{74}$$

This has the advantage of looking like a flat-space Dirac equation with an interaction term. Hence, much of the machinary of quantum theory in Minkowski space may be applied. However, the interaction term hides one significant feature: it is not Hermitian at the origin due to the presence of the singularity.

3.2.2 Current

Below we show the existence of a conserved four-current on a curved space-time. Starting from the Dirac equation (225) a conservation law can be found by considering

$$\psi^\dagger\gamma^0\left[ig^\mu\hat{D}_\mu\psi\right]-\left[ig^\mu\hat{D}_\mu\psi\right]^\dagger\gamma^0\psi=0, \tag{75}$$

where † denotes Hermitian conjugation. Assuming the torsion is zero (i.e. the connection is symmetric) we may make use of the identity

$$(-g)^{-1/2}\partial_\mu\left((-g)^{1/2}g^\mu\right)+\Omega_\mu g^\mu-g^\mu\Omega_\mu=0, \tag{76}$$

to rewrite equation (75) as

$$(-g)^{-1/2}\partial_\mu\left((-g)^{1/2}\bar{\psi}g^\mu\psi\right)=0, \tag{77}$$

where $\bar{\psi}$ is the Dirac adjoint, $\bar{\psi}=\psi^\dagger\gamma_0$. We may therefore define a conserved four-current J^μ satisfying

$$J^\mu{}_{;\mu}=0 \qquad \text{where} \qquad J^\mu=\bar{\psi}g^\mu\psi. \tag{78}$$

3.2.3 Separation of variables

To separate out the angular part of the wavefunction, we may use the two-component spherical spinors χ^μ_κ that are eigenvectors of the angular equation

$$(\boldsymbol{\sigma}\cdot\hat{\mathbf{L}}+1)\chi^\mu_\kappa=\kappa\chi^\mu_\kappa, \tag{79}$$

where $\hat{\mathbf{L}}=[\hat{L}_x,\hat{L}_y,\hat{L}_z]$ is the angular momentum operator, and the components of $\boldsymbol{\sigma}=[\sigma_x,\sigma_y,\sigma_z]$ are Pauli spin matrices. Angular states are labelled by the eigenvalue κ which is related to the overall angular momentum j by

$$\kappa=\pm(j+\tfrac{1}{2})=\begin{cases} l+1 & \text{when } j=l+\frac{1}{2} \\ -l & \text{when } j=l-\frac{1}{2}\end{cases}. \tag{80}$$

The spherical spinors are normalised so that

$$\int_0^{2\pi}d\phi\int_0^{\pi}\chi^{\mu\dagger}_\kappa\chi^{\mu'}_\kappa\sin\theta d\theta=\delta_{\mu\mu'}. \tag{81}$$

The positive and negative κ spinors are related by

$$\sigma_r\chi^\mu_\kappa=\chi^\mu_{-\kappa}, \tag{82}$$

where $\sigma_r=r^{-1}\sum_i x^i\sigma_i$.

We may now look for separable solutions of the form

$$\psi=\frac{e^{-i\omega t}}{r}\begin{pmatrix}u_1(r)\chi^\mu_\kappa(\theta,\phi)\\ u_2(r)\chi^\mu_{-\kappa}(\theta,\phi)\end{pmatrix}. \tag{83}$$

Substitution of trial function (83) into the Dirac equation (225) leads to a pair of coupled first-order equations for the radial functions $u_1(r)$ and $u_2(r)$.

In the Painlevé-Gullstrand coordinate system we find

$$\left(1-\frac{2M}{r}\right)\begin{pmatrix}u_1'\\u_2'\end{pmatrix}=\begin{pmatrix}1 & \sqrt{\frac{2M}{r}}\\ \sqrt{\frac{2M}{r}} & 1\end{pmatrix}\begin{pmatrix}\kappa/r & i(\omega+\mu)-\frac{1}{4r}\sqrt{\frac{2M}{r}}\\ i(\omega-\mu)-\frac{1}{4r}\sqrt{\frac{2M}{r}} & -\kappa/r\end{pmatrix}\begin{pmatrix}u_1\\u_2\end{pmatrix}. \tag{84}$$

[***Exercise***: Show this!]

3.2.4 Flux conservation

Let us now examine the form of the probability current in PG coordinates. Of course, the components of J^μ are observer dependent; in the PG coordinate system the J^0 component corresponds to the probability current that would be measured by an observer in radial free fall.

After integrating over the angular variables, the radial probability density in PG coordinates may be written

$$r^2\rho(r)=r^2\int d\Omega J^t=(|u_1|^2+|u_2|^2)e^{-i(\omega-\omega^*)t}, \tag{85}$$

and the radial probability flux is

$$r^2 j^r(r)=r^2\int d\Omega J^r=\left((u_1u_2^*+u_2u_1^*)-\sqrt{\frac{2M}{r}}(|u_1|^2+|u_2|^2)\right)e^{-i(\omega-\omega^*)t}. \tag{86}$$

[***Exercise***: Show this]. Conservation of flux for the Dirac equation may be summarised in the relation

$$\frac{\partial}{\partial t}\left(r^2\rho\right)=-\frac{\partial}{\partial r}\left(r^2 j^r\right). \tag{87}$$

3.2.5 Behaviour near the origin

Let us now consider the asymptotic limit $r\to 0$. Sufficiently close to the origin, we need only consider the lowest power of r on the right-hand side of (84), which in this case arises from the product of $\sqrt{2M/r}$ and $-\sqrt{2M/r}(4r)^{-1}$. This implies that

$$\frac{d}{dr}\begin{pmatrix}u_1\\u_2\end{pmatrix}\approx\frac{1}{4r}\begin{pmatrix}u_1\\u_2\end{pmatrix} \tag{88}$$

This makes it clear that both solutions u_1, u_2 go to the origin as $r^{1/4}$. From the assumed form of the separable solution, (83), all solutions diverge as $r^{-3/4}$ close to $r=0$, and so the probability density goes as $r^{-3/2}$. This is not a problem for normalisability however, since the integrated probability density is finite, as the lower limit of the integral $\int_0 drr^2r^{-3/2}=\left[(2/3)r^{3/2}\right]_0=0$ is zero.

The radial flux through a sphere of radius r is well-defined in the limit $r\to 0$

$$\lim_{r\to 0}\left(r^2 j^r\right)=-\lim_{r\to 0}\sqrt{\frac{2M}{r}}(|u_1|^2+|u_2|^2)=-\text{const.} \tag{89}$$

Hence a finite flux of probability density leaves the system at the origin.

To see this in another way, let us consider the Dirac equation in Hamiltonian form (with dimensionful constants $\hbar$ and c reinserted for physical clarity),

$$i\frac{\partial\psi}{\partial t} = -i\hat{\gamma}^0\hat{\gamma}^i\frac{\partial\psi}{\partial x^i} + m\hat{\gamma}^0\psi + \hat{H}_I\psi \tag{90}$$

where

$$\hat{H}_I\psi = i\sqrt{\frac{2M}{r}}\left(\frac{\partial}{\partial r} + \frac{3}{4r}\right)\psi. \tag{91}$$

The 'energy' E associated with the interaction term can be found through the integral

$$E = \int d^3x\psi^\dagger\hat{H}_I(\psi) = i\sqrt{2M}\int d\Omega\int_0^\infty drr^{3/4}\psi^\dagger\partial_r(r^{3/4}\psi). \tag{92}$$

Let us further assume that the wavefunction is normalised, $\int d^3x\psi^\dagger\hat{H}_I(\psi) = 1$. Integrating the equation once by parts with respect to r yields

$$E = i\sqrt{2M}\int d\Omega\left[r^{3/2}\psi^\dagger\psi\right]_0^\infty + \Delta E^\dagger. \tag{93}$$

If the state can be normalised, the boundary term goes to zero as $r\to\infty$, but does not disappear at the lower limit $r = 0$. As have seen, all wavefunctions go as $\psi\propto r^{-3/4}$ sufficiently close to the origin. The imaginary part of the energy is therefore finite and well-defined,

$$\mathrm{Im}(E) = -\tfrac{i}{2}(E - E^*) = -\tfrac{1}{2}\sqrt{2M}\lim_{r\to0}\int d\Omega\, r^{3/2}\psi^\dagger\psi \tag{94}$$

4 Time-Dependent Wave Mechanics

In this section we consider the response of a black hole to an initial perturbation. The black hole leaves a distinctive imprint on the scattered signal. It turns out that the black hole has certain resonant modes – called quasi-normal modes (QNMs) – whose frequency and decay time depend only on the black hole parameters (M, J, Q) and not on the specifics of the initial perturbation. It is hoped that these quasi-normal mode frequencies will be observed at gravitational wave detectors. A typical astrophysical scenario that would produce large amounts of gravitational waves is a black hole in the act of swallowing a neutron star at the endpoint of binary evolution. To accurately model this process, the full non-linear field equations must be solved. Nevertheless, the results of the linearized analysis provide a surprisingly accurate approximation to the full signal. To see the qualititative features, we consider only the scalar field here.

4.1 Wavefront scattering

One simple way to visualise a perturbation of a black hole is to model the evolution of the wave fronts by solving the geodesic equations for null rays. Figure 4 shows the results of a 1+2 time-domain simulation recently conducted by a student at UCD.

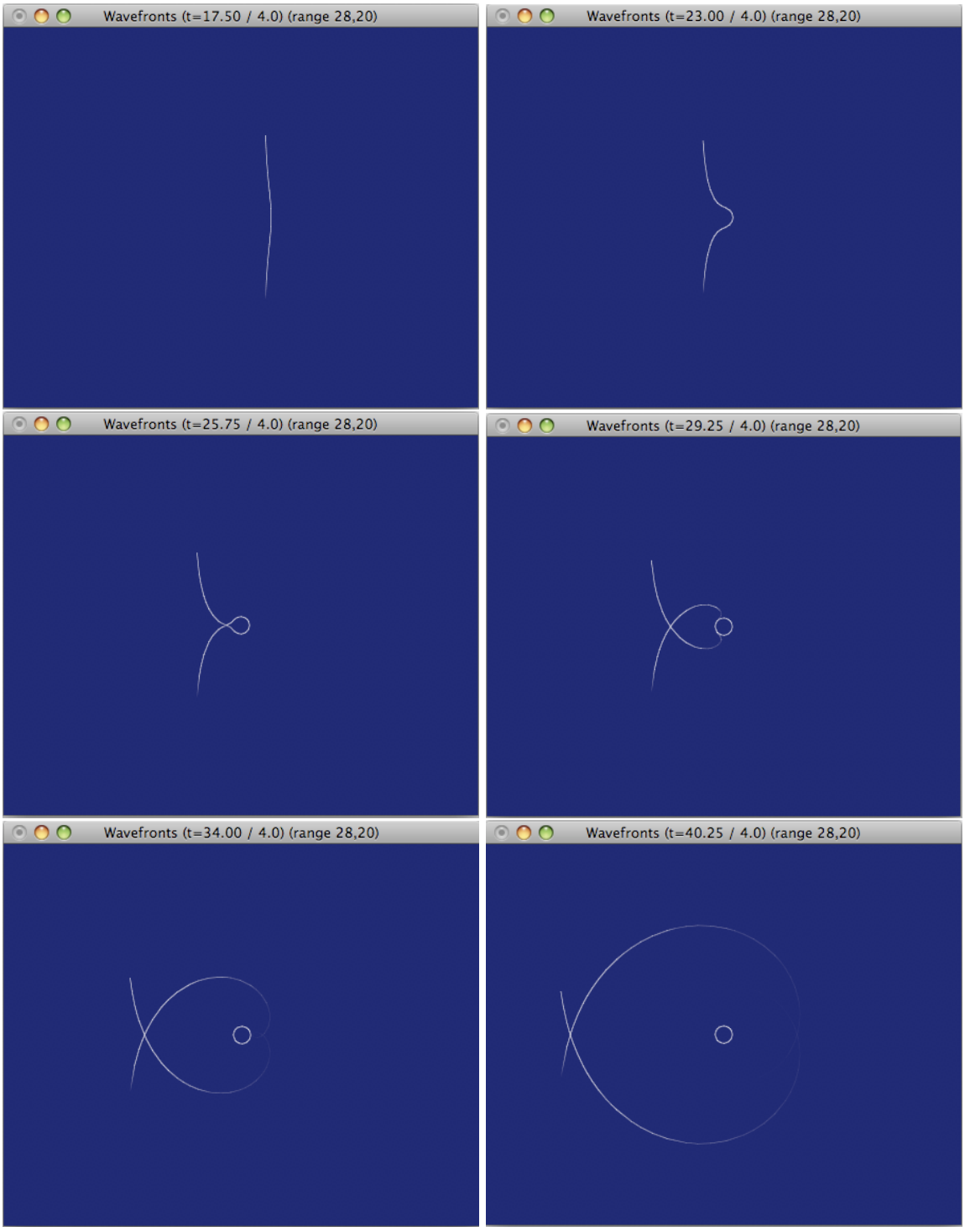

Figure 4: *Wave front scattering from a black hole.* The line shows the position of the wavefront at constant Schwarzschild coordinate time t. Results from code developed by Kirill Ignatiev, 2008 (School of Mathematical Sciences, UCD, Dublin [report in preparation]).

4.2 Wavepacket scattering

Let us imagine a simple scenario where a Gaussian wavepacket impinges upon a Schwarzschild hole. It is straightforward enough to pick a particular l, m mode, and integrate the $1+1$ wave equation

$$\frac{\partial^2 \phi_l}{\partial t^2} - \frac{\partial^2 \phi_l}{\partial r_*^2} + V_l(r_*)\phi_l = 0 \tag{95}$$

using a finite-difference method. Of course, the response depends on the width and speed of the incoming wavepacket. In a classic paper in the 1970s, Vishveshwara [19] tried bombarding a Schwarzschild hole with a range of wave packets of differing widths. He found that the response had some universal features.

Figure 6 shows a recreation of the scattering simulation. The black line shows the effective potential (for a massless wave). The blue line shows the scalar field. At $t = 0$, we start with a narrow Gaussian wavepacket approaching the hole. As it approaches, some flux is backscattered by the tail of the potential. As the wavepacket crosses the peak of the barrier, oscillations are induced. Some of the wavepacket is transmitted, and some is reflected. The proportion that is absorbed depends chiefly on the central frequency of the initial wavepacket.

The signal detected by an observer in the far-field region evolves with time. The response undergoes three distinct stages of evolution. First, the observer sees radiation backscattered from the tail of the potential. Next, the signal is dominated by an oscillatory component with a well-defined frequency and decay rate. Finally, the signal decays according to a power law. These three stages are shown clearly in Fig. 6. There is particular interest in the intermediate stage of *quasinormal-mode ringing*. The response at this stage resembles the 'pure tones of a bell' — the frequency and decay time depend not on the details of the initial perturbation, but only on the parameters of the black hole.

The quasinormal mode ringing is excited by the passage of the wavepacket across the maximum of the effective potential. The presence of a potential maximum (correspondingly, an unstable photon orbit) is a feature unique to black holes: hence detection of a QNM frequencies in a GW signal would be a clear signature of black holes.

4.3 Quasi-Normal Modes

Which begs the questions: what precisely are QNMs and how may we determine their frequencies?

Quasi-normal modes are solutions to the radial wave equation (41) which satisfy the boundary conditions

$$u_l(r) = \begin{cases} e^{-i\omega r_*}, & r_* \to -\infty, \\ e^{+i\omega r_*} & , \quad r_* \to \infty. \end{cases} \tag{96}$$

In other words, QNMs are ingoing at the horizon and outgoing at infinity. Clearly, they act a bit like resonant modes since an outgoing signal can be excited by an 'infinitessimal' ingoing perturbation. But, the QNM frequencies ω are complex. The negative imaginary part of the frequency determines the decay rate. Since flux is radiated through the horizon and away to infinity, it is natural that these modes decay with time.

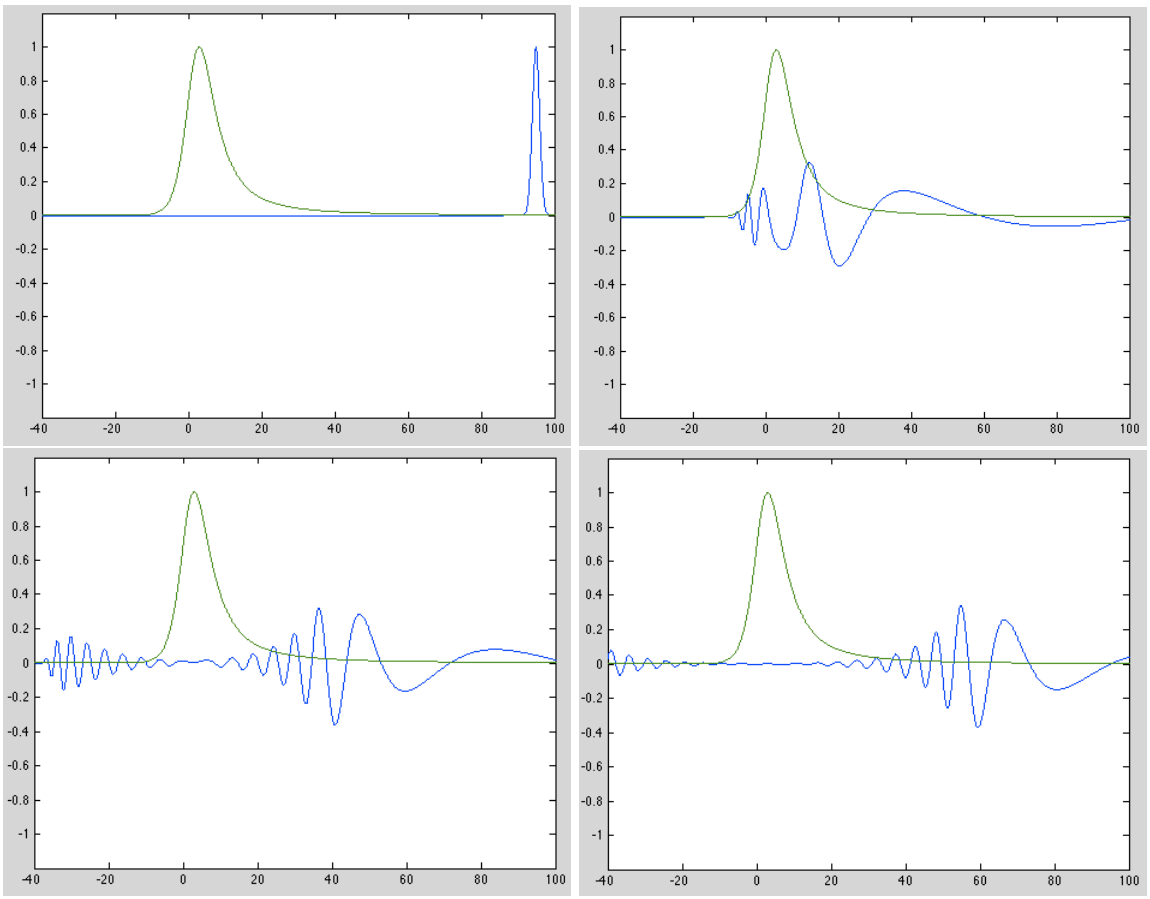

Figure 5: *Vishveshwara's scattering simulation: A wave packet scattering from a black hole.* The black line shows the effective potential barrier, and the blue line shows the scalar field. The graphs illustrate the evolution in time of a Gaussian wavepacket impinging upon the hole.

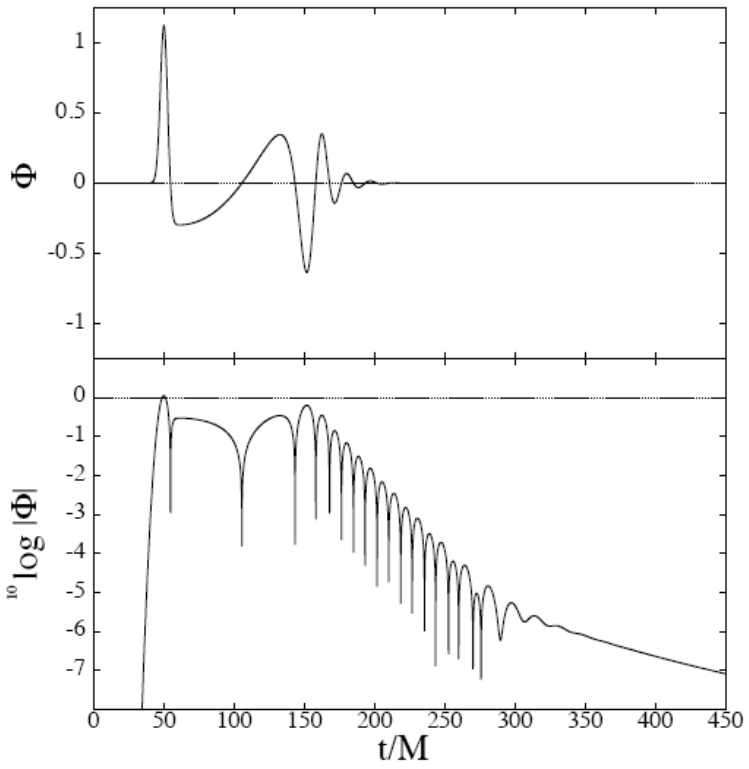

Figure 6: *The time-dependent response to wavepacket scattering at fixed position far from the hole.* This figure is taken from Andersson & Jensen (2001) [gr-qc/0011025], who comment "The response of a Schwarzschild black hole as a Gaussian wavepacket of scalar waves impinges upon it. The first bump (at $t = 50M$) is the initial Gaussian passing by the observer on its way towards the black hole. Quasinormal-mode ringing clearly dominates the signal after $t \sim 150M$. At very late times (after $t \sim 300M$) the signal is dominated by a power-law fall-off with time. This late time tail arises because of backscattering off of the weak potential in the far zone. As such, it is not an effect exclusive to black holes. A similiar tail will be present also for perturbed stars."

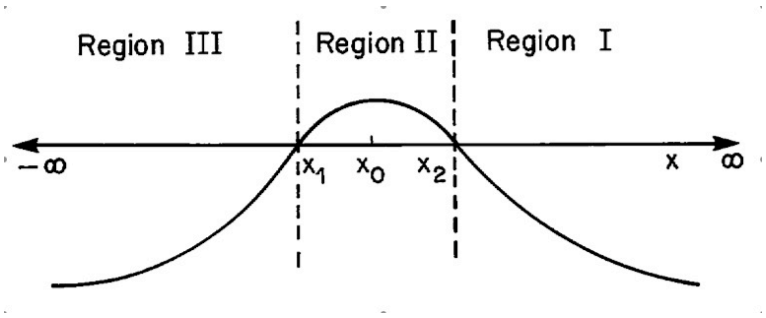

Figure 7: *The WKB approximation.* A wave of frequency ω interacts with the peak of the potential barrier. Three zones are shown: in I and III, $|\omega| < V(r_*)$, whereas in II $|\omega < V(r_*)$. A solution is matched together at the boundaries.

The QNM spectrum can be approximated using semi-analytic methods. For example, the WKB method may be applied [17]. We may attempt to match up asymptotic solutions across the potential barrier, as illustrated in Fig. 7. In regions I and III, the asymptotic solutions are

$$\Phi_I(r_*) = Q^{-1/4}(r_*)\, \exp\left(+i \int_{x_2}^{r_*} Q^{1/2}(x)dx\right) \tag{97}$$

$$\Phi_{III}(r_*) = Q^{-1/4}(r_*)\, \exp\left(-i \int_{r_*}^{x_1} Q^{1/2}(x)dx\right) \tag{98}$$

where $Q(r_*) = \omega^2 - V(r)$. Note that these asymptotic forms are only valid far from the matching points (e.g. $Q(r^*)(r^* - x_2)^2 \gg 1$). [***Exercise***: Show that Φ_I satisfies the equation $\Phi''/\Phi = Q + 5(Q'/4Q)^2 - Q''/4Q$].

Near the peak of the potential, the function $Q(r_*)$ can be approximated by a parabola, $Q = Q_0 + Q_0''(r^* - r_0^*)^2$. The radial equation can be written in a standard form,

$$\frac{d^2\Phi_{II}}{dt^2} + \left(\nu + \tfrac{1}{2} - \tfrac{1}{4}t^2\right)\Phi = 0, \tag{99}$$

by making the definitions

$$t = (4k)^{1/4} e^{i\pi/4}(r^* - r_0^*), \qquad k = Q_0''/2, \qquad \nu + \tfrac{1}{2} = -iQ_0/(2Q_0'')^{1/2}. \tag{100}$$

The solutions to (99) are parabolic cylinder functions $D_\nu(t)$, and the general solution is $\Phi_{II} = AD_\nu(t) + BD_{-\nu-1}(it)$. By considering the asymptotic form of the parabolic cylinder functions in the limits $t \to \infty$ and $t \to -\infty$ it can be shown that Φ_{II} will only match Φ_I and Φ_{III} if $\Gamma(-\nu) = -\infty$. [***Exercise***: Show this]. Hence ν is a non-negative integer, and so the QNMs have a discrete spectrum approximated by

$$\omega^2 = V(r_0) - i(n + \tfrac{1}{2})\left(-2\, \frac{d^2V}{dr_*^2}\bigg|_{r=r_0}\right)^{1/2} \tag{101}$$

where r_0 is the position of the peak of the potential.

To compute the QNMs more accurately, a numerical method may be employed. Below I briefly outline a method of continued fractions [12] which is both fast and numerically stable.

Let us make a substitution which has the desired properties at the horizon (ingoing) and infinity (outgoing). In the limit $r \to 2M$, we have $r_* \to 2M \ln(r/2M - 1)$, hence we start with the ansatz

$$u_l(r) = (r-2m)^{\rho} r^{-2\rho} e^{-\rho(r-2M)/2M} \sum_{n=0}^{\infty} a_n \left(\frac{r-2m}{r}\right)^n \tag{102}$$

where $\rho = -2im\omega$. Substituting this ansatz into the radial equation (41), we find the series coefficients a_n satisfy a three-term recurrence relation,

$$\alpha_n a_{n+1} + \beta_n a_n + \gamma_n a_{n-1} = 0, \tag{103}$$

where

$$\alpha_n = n^2 + 2n(\rho+1) + 2\rho + 1 \tag{104}$$

$$\beta_n = -[2n^2 + 2n(4\rho+1) + 8\rho^2 + 4\rho + l(l+1) + 1] \tag{105}$$

$$\gamma_n = n^2 + 4n\rho + 4\rho^2 \tag{106}$$

The frequency ω corresponds to a QNM if and only if the sum $\sum a_n$ converges. This requirement translates into a continued-fraction equation involving the coefficients α, β and γ

$$\beta_0 - \frac{\alpha_0\gamma_1}{\beta_1 -}\frac{\alpha_1\gamma_2}{\beta_2 -}\frac{\alpha_2\gamma_3}{\beta_3 -}\ldots = 0. \tag{107}$$

The roots of this equation yield the QNM frequencies. In practice, it is better to solve an inversion of this equation when looking for higher-order modes. The roots can be found with a numerical root-finding algorithm.

The numerically-determined QNM frequencies are shown in Fig. 9. The most physically-significant mode is the mode that decays most slowly – in other words, the least-damped mode with the smallest negative imaginary component (i.e. $\min|\mathrm{Im}(\omega)|$). This 'fundamental' mode dominates the time-domain signal shown in Fig. 6.

4.4 Green's Function Analysis

A clearer picture of the dynamic response of a black hole to perturbation may be obtained via a Green's function approach. In this section, we consider the evolution of the field as an initial value problem. Instead of specifying some arbitary initial condition we instead seek to determine the general features of the response by examining the propagator (i.e. the Green's function).

The time-evolution of a wave-field $\Phi_l(r_*, t)$ is given by

$$\Phi_l(r_*, t) = \int G(r_*, y, t)\partial_t \Phi_l(y, 0)dy + \int \partial_t G(r_*, y, t)\Phi_l(y, 0)dy. \tag{108}$$

The retarded Green's function is defined by

$$\left[\frac{\partial^2}{\partial t^2} - \frac{\partial^2}{\partial r_*^2} + V(r)\right] G(r_*, y, t) = \delta(t)\delta(r_* - y), \tag{109}$$

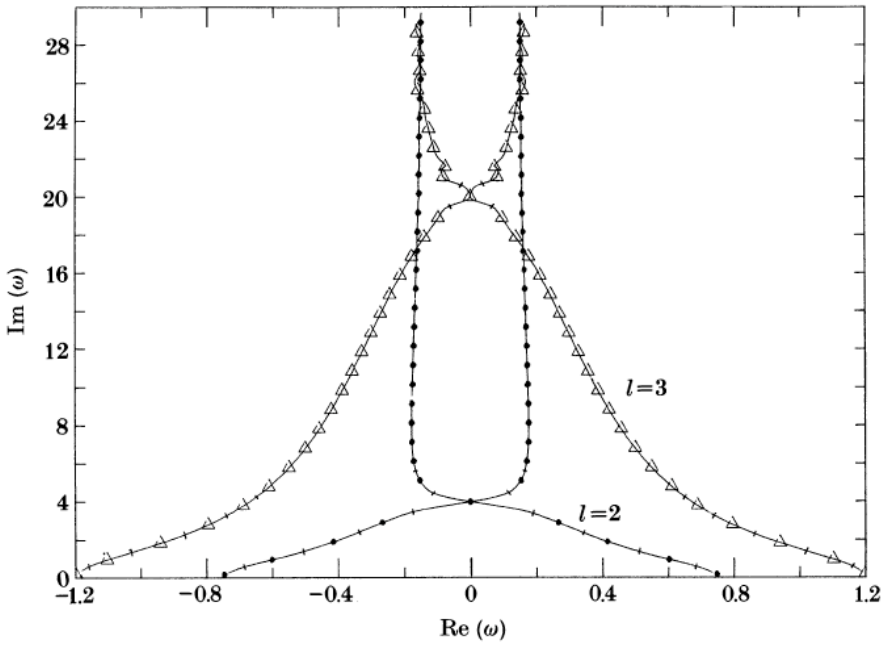

Figure 8: *The Quasi-Normal Mode Spectrum.* This plot is taken from Fig. 1, E.W. Leaver, *Proc. R. Soc. Lond. A* **402**, 285–298 (1985). It shows the quasi-normal mode frequencies of the gravitational field of the Schw. BH., for the $l = 2$ and $l = 3$ angular modes. Note that with our conventions, the y-axis should read $-\mathrm{Im}(\omega)$.

and the condition $G(r_*, y, t) = 0$ for $t \leq 0$. The ingoing boundary condition at the horizon is imposed by demanding

$$\frac{\partial G}{\partial r_*} + i\omega G = 0, \qquad r \to 2M \tag{110}$$

and the outgoing condition at infinity is imposed by demanding

$$\frac{\partial G}{\partial r_*} - i\omega G = 0, \qquad r \to \infty. \tag{111}$$

We may now perform a Fourier transform of G:

$$\hat{G}(r_*, y, \omega) = \int_{0^-}^{\infty} G(r_*, y, t) e^{i\omega t} dt \tag{112}$$

The transform is well defined as long as $\mathrm{Im}\omega \geq 0$, and the inversion formula is

$$G(r_*, y, t) = \frac{1}{2\pi} \int_{-\infty+ic}^{\infty+ic} \hat{G}(r_*, y, \omega) e^{-i\omega t} d\omega \tag{113}$$

where c is a positive real number. [***Exercise***: Prove that this expression is indeed the inverse].

The Green's function $\hat{G}(r_*, y, \omega)$ can be expressed in terms of two linearly-independent solutions to the homogenous equation. In order to obtain the correct boundary conditions on G, we will make use of the two solutions 'in' and 'up'. The 'in' solution is purely ingoing at the horizon, whereas the 'up' solution is purely outgoing at infinity.

$$\phi_l^{(\mathrm{in})} \sim \begin{cases} e^{-i\omega r_*}, & r_* \to -\infty, \\ A_{\mathrm{in}} e^{-i\omega r_*} + A_{\mathrm{out}} e^{+i\omega r_*}, & r_* \to +\infty, \end{cases} \tag{114}$$

and

$$\phi_l^{(\mathrm{up})} \sim \begin{cases} B_{\mathrm{in}} e^{-i\omega r_*} + B_{\mathrm{out}} e^{+i\omega r_*}, & r_* \to -\infty, \\ e^{+i\omega r_*}, & r_* \to +\infty. \end{cases} \tag{115}$$

Here, A_{in}, A_{out}, B_{in} and B_{out} are complex constants which depend on the frequency of the mode under consideration, ω. boundary conditions are illustrated on a Penrose-Carter conformal diagram in Fig. **??**.

The Green's function is

$$\hat{G}(r_*, y, \omega) = -\frac{1}{W} \begin{cases} \phi_l^{(\mathrm{in})}(r_*)\phi_l^{(\mathrm{up})}(y), & r_* < y, \\ \phi_l^{(\mathrm{up})}(r_*)\phi_l^{(\mathrm{in})}(y), & r_* > y \end{cases} \tag{116}$$

Note that the properties of $\phi_l^{(\mathrm{in})}$ and $\phi_l^{(\mathrm{up})}$ ensure that the boundary conditions (110) and (111) are met. Here W is the Wronskian given by

$$W = \phi_l^{(\mathrm{in})} \frac{d\phi_l^{(\mathrm{up})}}{dr_*} - \phi_l^{(\mathrm{up})} \frac{d\phi_l^{(\mathrm{in})}}{dr_*} = 2i\omega A_{\mathrm{in}}. \tag{117}$$

4.4.1 Contour integration

In principle the initial value problem can be solved by direct numerical integration. However, there is an alternative approach which clearly reveals the origin of the phases of evolution seen in the dynamical response of Fig. 6. In this approach, we compute the contour integral (113) using Cauchy's theorem. For $t > 0$, the contour can be closed in the lower half-plane, provided as we integrate around a branch cut. The closed contour and the branch cut are shown in Fig. 9. The contour encloses 'poles' of the Green's function $\hat{G}$ where the Wronskian W (117) is zero. These poles are none other than the QNM frequencies!

The three phases of time evolution correspond to three parts of the contour diagram. The initial response arises from the high-frequency arcs that complete the contour. The intermediate ringing is due to the contribution from the residues at the poles. The late-time power law decay arises from the integral along the branch cut.

4.5 Bound States

Electromagnetic and gravitational waves are massless; Dirac perturbations are not. It is simple enough to include a field mass in the wave equation and we might ask: what are the consequences?

As we saw in Sec. (**??**), field mass may create a local minimum in the effective potential. A minimum corresponds to the existence of a stable circular orbit. It raises the possibility of "bound states" localized in the potential well. In other words, like the hydrogen atom, a black hole may have a spectrum of bound state energy levels. These states cannot be unitary however, since they would quantum-tunnel through the potential barrier into the near-horizon region. Such states will decay exponentially with time, as flux is lost through the horizon.

The field mass μ corresponds to a length scale: the Compton wavelengh $\lambda = h/\mu c$. Let us define a dimensionless mass coupling α_G to be proportional to the ratio of the Compton

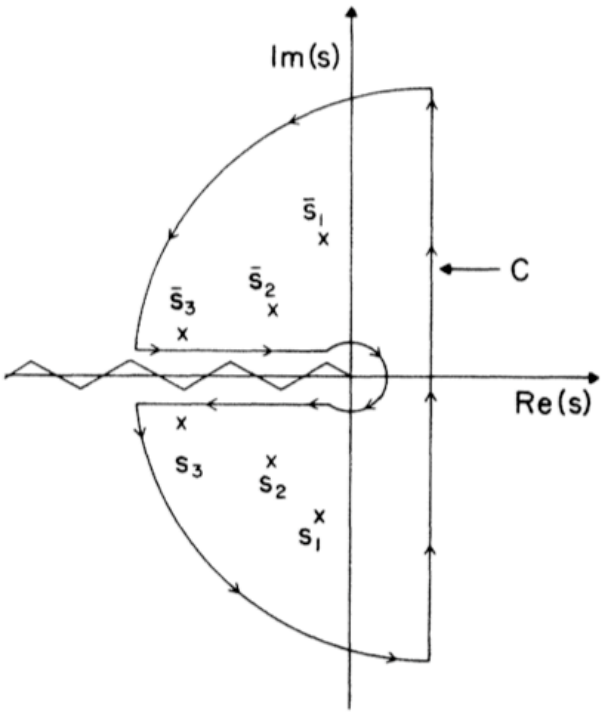

Figure 9: *The Contour Integral.* This plot is taken from Fig. 1, E.W. Leaver, *Phys. Rev. D* **34**, 384 (1986). It shows a complete contour of integration that encloses all the QNM frequencies. Here, $s = i\omega^*$.

wavelength of the particle to the horizon size of the hole,

$$\alpha_G = \frac{\pi r_s}{\lambda} = \frac{GM\mu}{\hbar c}. \tag{118}$$

A local minimum in the potential (and thus quasi-stable states) is only possible in the regime $\alpha_G \lesssim l$, where l is the angular momentum of the mode.

For astrophysical black holes coupled to known matter fields, $\alpha_G \gg 1$. For instance, for a solar-mass black hole $M \sim 2 \times 10^{30}$ kg coupled to the electron mass $m_e \sim 9.11 \times 10^{-31}$kg, we find $\alpha_G \sim 10^{14}$. It makes little sense to talk about an $l \sim 10^{14}$ mode; far better to examine the local dynamics of the field. However, if *primordial* black holes were created in the early universe they may have much smaller masses. A value of $\alpha_G \sim 1$ corresponds to a BH of mass 10^{15} kg coupled to the electron field; or a BH of mass 10^{21} kg coupled to a neutrino field with (hypothetical) mass 0.01eV.

Like QNMs, bound states satisfy a pair of boundary conditions. Unlike QNMs, bound states tend to zero at spatial infinity. That is,

$$u_l \sim \begin{cases} e^{-i\omega r_*}, & r_* \to -\infty \\ Ae^{-qr_*}, & r_* \to +\infty \end{cases} \tag{119}$$

where $q = \sqrt{\mu^2 - \omega^2}$. The frequency ω has a negative imaginary part, and thus the state decays with time. (To ensure convergence in the far-field, we choose the square root so that $-\mathrm{Re}(q) < 0$).

The method of continued fractions can be modified to calculate bound state frequencies, as we show in the next section. First, let us examine the spectrum in the limit $\alpha_G/l \ll 1$.

4.5.1 Non-relativistic bound state spectrum

In this section it is shown that in the non-relativistic limit, the frequency spectrum of the scalar field bound to a Schwarzschild black hole has a hydrogen-like spectrum,

$$\hbar\omega_n \approx \left(1 - \frac{M^2\mu^2}{2\bar{n}^2}\right)\mu c^2, \tag{120}$$

where $\bar{n} \in \mathbb{N}^+$ is the principal quantum number.

Let us begin by considering the Schwarzschild spacetime described by Painlevé-Gullstrand (PG) coordinates. It is straightforward to show that the massive Klein-Gordon equation in PG coordinates can be written

$$\left(\partial_t - \sqrt{2M/r}\,\partial_r\right)^2\Phi - \frac{3}{2r}\sqrt{\frac{2M}{r}}\left(\partial_t - \sqrt{2M/r}\,\partial_r\right)\Phi - \boldsymbol{\nabla}^2\Phi + \mu^2\Phi = 0 \tag{121}$$

where $\boldsymbol{\nabla}^2$ is the 3D Laplacian operator [***Exercise***].

To effect a non-relativistic reduction, we split the field Φ into two components χ_1 and χ_2, defined by

$$\chi_1 = \tfrac{1}{2}\left(\Phi + \frac{i}{\mu}\left(\partial_t - \sqrt{2M/r}\,\partial_r\right)\Phi\right), \tag{122}$$

$$\chi_2 = \tfrac{1}{2}\left(\Phi - \frac{i}{\mu}\left(\partial_t - \sqrt{2M/r}\,\partial_r\right)\Phi\right), \tag{123}$$

so that

$$\chi_1 + \chi_2 = \Phi \qquad \text{and} \qquad \chi_1 - \chi_2 = \frac{i}{\mu}\left(\partial_t - \sqrt{2M/r}\,\partial_r\right)\Phi. \tag{124}$$

This decomposition leads to the pair of coupled equations,

$$(i\partial_t - \mu)\,\chi_1 = -\frac{1}{2\mu}\boldsymbol{\nabla}^2(\chi_1+\chi_2) + i\sqrt{2M/r}\,\partial_r\chi_1 + \frac{3i}{4r}\sqrt{2M/r}\,(\chi_1-\chi_2), \tag{125}$$

$$(i\partial_t + \mu)\,\chi_2 = +\frac{1}{2\mu}\boldsymbol{\nabla}^2(\chi_1+\chi_2) + i\sqrt{2M/r}\,\partial_r\chi_2 + \frac{3i}{4r}\sqrt{2M/r}\,(\chi_2-\chi_1). \tag{126}$$

In the non-relativistic limit, we make the assumption that $\omega \sim \mu$ and the approximation $\chi_2 \ll \chi_1$. Equally well, we could make the assumption that $\omega \sim -\mu$ to recover the non-relativistic antiparticle spectrum. This assumption leads to the Schrödinger equation

$$E_{NR}\chi_1 = -\frac{1}{2\mu}\boldsymbol{\nabla}^2\chi_1 + i\sqrt{\frac{2M}{r}}\left(\partial_r + \frac{3}{4r}\right)\chi_1 \tag{127}$$

where $E_{NR} = \omega - \mu$. With a simple substitution, $\chi_1 = \psi\exp(i\mu\sqrt{8Mr})$, equation (127) can be transformed to the familiar form

$$E_{NR}\psi = -\frac{1}{2\mu}\boldsymbol{\nabla}^2\psi - \frac{M\mu}{r}\psi. \tag{128}$$

This is the hydrogenic Schrödinger equation, but with the fine-structure constant $\alpha_{EM} = e^2/4\pi\epsilon_0\hbar c$ replaced by the gravitational coupling $\alpha_G = GM\mu/\hbar c$. Hence the non-relativistic wavefunctions are hydrogenic, and the energy levels are given by (120).

4.5.2 Continued Fraction Method

It is possible to adapt the QNM continued-method to numerically determine the bound state frequencies. Let us look for a solution of the form

$$u_l(r) = (r-2M)^{-i\sigma} r^{i\sigma+\chi} e^{qr} \sum_{n=0}^{\infty} a_n \left(\frac{r-2M}{r}\right)^n \tag{129}$$

where

$$\sigma = 2M\omega, \qquad q = \pm\sqrt{\mu^2-\omega^2}, \qquad \text{and} \qquad \chi = \frac{\mu^2-2\omega^2}{q}. \tag{130}$$

[***Exercise***: Verify that this ansatz satisfies the pair of boundary conditions (119) if the series is convergent].

The choice of the sign of the real part of q determines the behaviour of the wavefunction as $r \to \infty$. If $\mathrm{Re}(q) > 0$, the solution diverges towards infinity, whereas if $\mathrm{Re}(q) < 0$ the solution tends to zero. Therefore, the same method can be applied to look for both quasinormal modes (by choosing $\mathrm{Re}(q) > 0$) *and* the bound state modes (by choosing $\mathrm{Re}(q) < 0$).

Substituting (129) into the radial equation (41) yields a three-term recurrence relation for the coefficients a_n. We find

$$\alpha_0 a_1 + \beta_0 a_0 = 0 \tag{131}$$

$$\alpha_n a_{n+1} + \beta_n a_n + \gamma_n a_{n-1} = 0, \qquad n > 0, \quad n \in \mathbb{N}^+, \tag{132}$$

where

$$\alpha_n = n^2 + (c_0+1)n + c_0, \tag{133}$$

$$\beta_n = -2n^2 + c_1 n + c_3, \tag{134}$$

$$\gamma_n = n^2 + c_2 n + c_4. \tag{135}$$

The constants c_0, c_1, c_2, c_3 and c_4 are somewhat more complicated than in the massless case [12]. Explicitly,

$$c_0 = 1 - 4i\omega, \tag{136}$$

$$c_1 = -2 + 8i(\omega - iq) - \frac{2(\omega^2+q^2)}{q}, \tag{137}$$

$$c_2 = -4i\omega - \frac{2(q^2-\omega^2)}{q}, \tag{138}$$

$$c_3 = \frac{2i(\omega-iq)^3}{q} + 2(\omega-iq)^2 - l(l+1) - 1 - \frac{(\omega-iq)^2}{q} + 2q + 2i\omega\left(\frac{(\omega-iq)^2}{q} + 1\right), \tag{139}$$

$$c_4 = \frac{(\omega-iq)^4}{q^2}. \tag{140}$$

Note that here I have set $M = 1$ for convenience (hence ω and q are expressed in units of M^{-1}). In the massless limit ($\mu = 0$, $q = i\omega$), equations (136)—(140) should reduce to (**??**) [***Exercise***: check this is true!]. To find the bound state frequencies, we may follow the method outlined in Sec. 4.3.

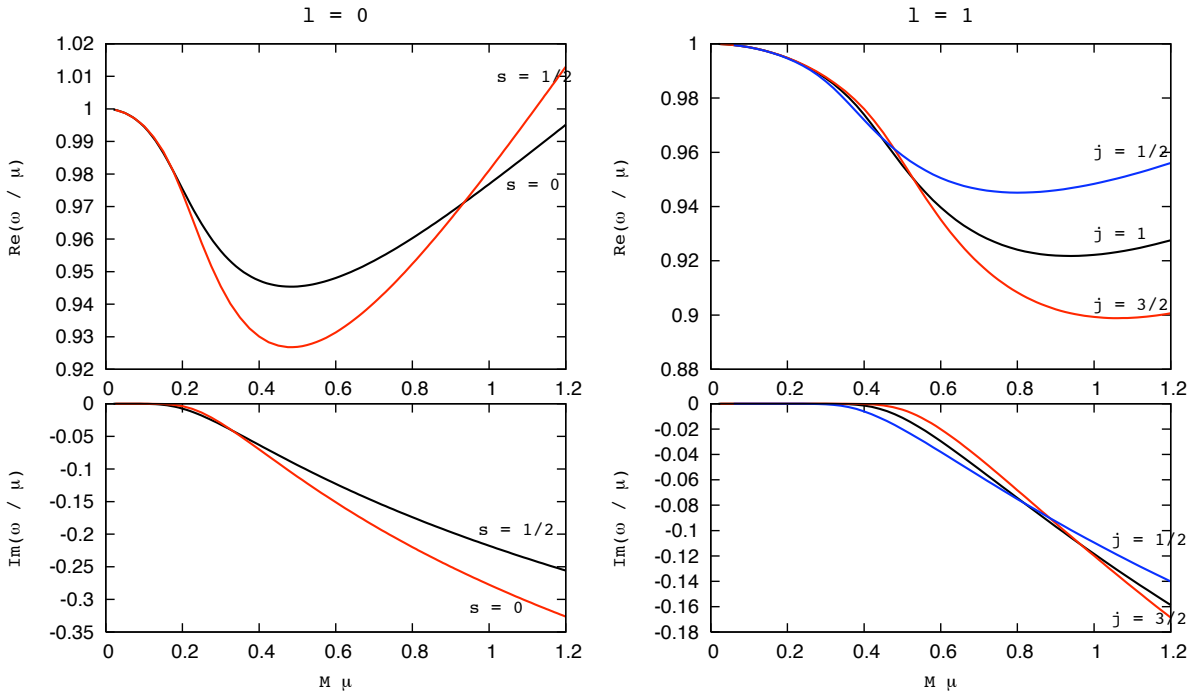

Figure 10: *Scalar* ($s = 0$) *and spinor* ($s = 1/2$) *bound state frequencies of the Schwarzschild hole.* The upper plots show the real component of energy (i.e. the oscillation frequency), and the bottom plots show the imaginary component (i.e. the decay frequency), as a function of gravitational mass coupling $GM\mu/\hbar c$. The left plots compare the $l = 0$ scalar ground state with the $j = 1/2$ spinor ground state. The right plots compare the $l = 1$ (scalar) and the $j = 1/2$ and $j = 3/2$ (spinor) levels.

Figure 10 compares the spectra of the massive Klein-Gordon and Dirac fields on the Schwarzschild background. In the limit $M\mu \ll 1$, the spectra follow equation (120). As $M\mu$ is increased, the frequency develops a non-negligible negative imaginary component. At higher couplings, the spin has a significant effect on the frequency levels. In the spin-half case, the $j = l \pm 1/2$ degeneracy is split by the black hole interaction. For couplings $M\mu \gtrsim 0.3$, the (negative) imaginary part of the energy is comparable to the field mass. This means that decay is extremely fast, similar to the Compton time. To put it another way, if $M\mu \gtrsim l$, the state lasts only a few multiples of the light-crossing time for the black hole.

Figure 11 shows the frequency spectrum for scalar states of higher angular momentum, up to $l = 8$. Again, the levels follow the hydrogenic $(1/\overline{n}^2)$ spectrum (120) in the regime $M\mu \ll l$. At low couplings, the states are quasi-stable. Decay dominates beyond about $M\mu \sim 0.3l$. At around $M\mu \sim 0.5(l+1)$ the real part of the energy reaches a minimum. The maximum 'binding energy' offered by this minimum increases with l, to around 12% of the rest mass energy for $l = 8$. It seems unlikely that this energy could be extracted from the black hole, since the state decays very rapidly (with a lifetime similar to the black hole light-crossing time).

Radial wavefunctions for the first three modes with $l = 0$ are shown in Fig. 12. These plots show the time-like component of the current as measured by an infalling observer. For $\alpha \ll 1$,

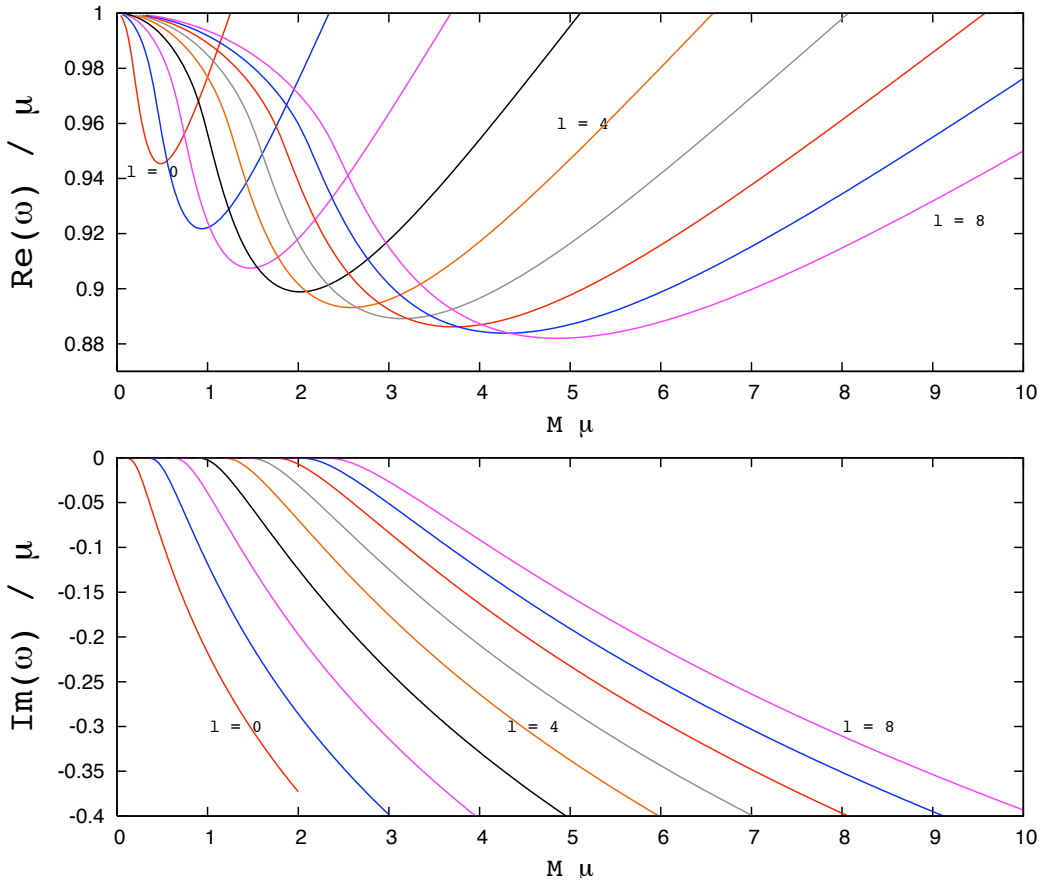

Figure 11: *The complex frequencies of the lowest-energy Schwarzschild bound states up to* $l = 8$. The top plot shows the oscillation frequency $\mathrm{Re}(\omega/\mu)$, and bottom plot shows the decay rate $\mathrm{Im}(\omega/\mu)$, as a function of the mass coupling $GM\mu/\hbar c$.

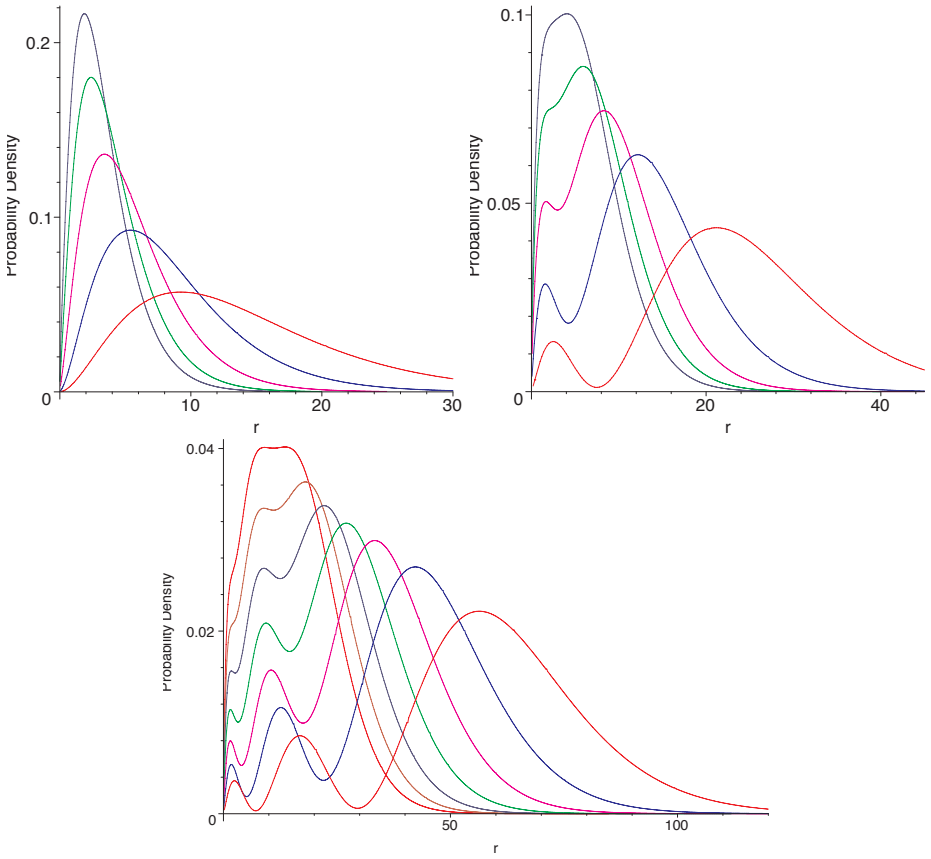

Figure 12: *S-state wavefunctions.* The top-left plot shows 1S wavefunctions in the range $0.1 \leq \alpha \leq 0.3$. The top-right and bottom plots show the 2S and 3S states in the ranges $\alpha = 0.2 - 0.6$ and $\alpha = 0.2 - 0.5$, respectively.

the wavefunctions are hydrogenic. At higher couplings, the peak of the wavefunction moves closer to the singularity and the nodal structure is washed out.

5 Time Independent Scattering and Absorption

In this section we consider a time-independent scattering scenario in which a long-lasting monochromatic wave impinges onto a black hole. The key physical quantities are:

- the absorption cross section σ_a
- the differential scattering cross section$d\sigma/d\Omega$
- the partial polarization (if the wave has spin), $\mathcal{P}$.

Scattering calculations are a standard part of quantum theory, and the methods can be adapted to the black hole case. Below I describe two standard approachs: a perturbation theory calculation and the partial wave method.

5.1 Perturbative Scattering Theory

This section describe the application of perturbation theory to the calculation of black hole scattering cross sections. Perturbation theory has played a key role in the development of quantum mechanics. Whilst it is relatively straightforward to write down equations that describe the propagation and interaction of relativistic quantum fields, it is altogether more difficult to solve them! Ultimately, a physical theory must prove itself by calculating physical quantities (for example, transition probabilities, scattering cross sections, etc.) for comparison with experiment. Perturbation theory is a crucial tool for such calculations.

The archetypal example of a successful application of perturbation theory to quantum mechanics is Feynman's formulation of Quantum Electrodynamics (QED). QED describes the interaction of relativistic electrons and positrons with the quantised electromagnetic field. Physical quantities such as the scattering amplitude can be expressed as Born series in the interaction parameter. That is,

$$\mathcal{M} = a_1\alpha + a_2\alpha^2 + a_2\alpha^3 + \ldots \tag{141}$$

where $\mathcal{M}$ is the scattering amplitude, α is the fine-structure constant, and the constant a_i is calculated by summing all Feynman diagrams containing i interactions between the fields. The perturbative method is particularly effective for QED because $\alpha \approx 1/137 \ll 1$, so relatively few terms are required in the Born series to obtain an accurate result. A great triumph for the theory came with the accurate confirmation of the Lamb shift observed in the hydrogen spectrum.

An early application of perturbation theory was to the scattering of high-energy electrons by nuclei. Following the publication of Dirac's equation in 1928, various authors applied Born's method to obtain a scattering cross section at first order,

$$\frac{d\sigma}{d\Omega} = \frac{Z^2e^4(1-v^2)}{4m^2\sin^4(\theta/2)}\left[1 - v^2\sin^2(\theta/2)\right], \tag{142}$$

which was in agreement with Mott's formula. Here, $v = p/\hbar\omega$ is the velocity of the incident electron in units of c.

The full Born series for the Schwarzschild black hole scattering cross section may be written as

$$\frac{d\sigma}{d\Omega} = \left(\frac{GM}{c^2}\right)^2\left[a_0(v,\theta) + M\omega a_1(v,\theta) + M^2\omega^2 a_2(v,\theta) + \ldots\right], \tag{143}$$

with $M\omega \equiv GM\omega/c^3$ as defined in chapter **??**, and $a_i(v,\theta)$ dimensionless functions. The perturbation series approach is most appropriate in the long-wavelength limit, when $M\omega \ll 1$.

There is a great deal of freedom in the choice of coordinate system used to describe the Schwarzschild solution. It makes sense to work with a horizon-penetrating coordinates, such as AEF or PG coordinates. However, the formal details of the perturbation calculation are quite different in these two systems. We would hope that physical quantities – i.e. the cross sections – would be coordinate-system independent (*gauge-invariant*). Here we show that the first-order cross section is the same AEF and PG coordinate systems, but this is far from a general proof of gauge-invariance!

5.1.1 Klein-Gordon scattering

Let us begin by reviewing the perturbation method for the Klein-Gordon field. For an introduction to spin-zero perturbation theory see, for example, chapter 8 in Greiner's textbook [9]. We start by assuming that the Klein-Gordon equation may be written as

$$\partial^\mu \partial_\mu \Phi + \mu^2 \Phi + \hat{B}\Phi = 0 \tag{144}$$

where $\partial^\mu \partial_\mu$ is the flat-space d'Alembertian, and the interaction term

$$\hat{B}\Phi = (-g)^{-1/2} \partial_\mu \left[(-g)^{1/2} \left(g^{\mu\nu} - \eta^{\mu\nu} \right) \partial_\nu \Phi \right] \tag{145}$$

is assumed to be in some sense 'small' (note that this assumption breaks down near the origin). Here, $\eta^{\mu\nu}$ is the Minkowski metric in the appropriate coordinate system. For example, in our case $\eta^{\mu\nu} = \text{diag}\left[1, -1, -r^2, -r^2 \sin^2\theta\right]$, and operator $\hat{B}$ includes t and r partial derivatives.

Let us assume harmonic time-dependence, so that $\hat{B}$ is a function of r only. The propagator (Green's function) Δ_G is defined by

$$\left[(\partial_\mu \partial^\mu)_{x_2} + \mu^2 + \hat{B}(x_2) \right] \Delta_G(x_2, x_1) = \delta^4(x_2 - x_1)\,. \tag{146}$$

and appropriate boundary conditions. The propagator may be expanded in a perturbation series,

$$\begin{aligned} \Delta_G(x_f, x_i) =& \Delta_F(x_f, x_i) - \int d^4x_1 \Delta_F(x_f, x_1) \hat{B}(x_1) \Delta_F(x_1, x_i) + \\ & \int\int d^4x_1 d^4x_2 \Delta_F(x_f, x_1) \hat{B}(x_1) \Delta_F(x_1, x_2) \hat{B}(x_2) \Delta_F(x_2, x_i) + \ldots \end{aligned} \tag{147}$$

where $\Delta_F(x_2, x_1)$ is the free-space Feynman propagator for the scalar particle. In momentum space this is

$$\Delta_F(x_2, x_1) = \int \frac{d^4k}{(2\pi)^4} \Delta_F(k) e^{-ik\cdot(x_2 - x_1)}, \qquad \Delta_F(k) = \frac{1}{k^2 - \mu^2}.. \tag{148}$$

If we wish to evaluate (148) explicitly, we must remember to construct the contour of integration so as to recover the correct causal behaviour. This can be done by adding a small imaginary part to the denominator. Instead, it is simpler to convert the whole calculation to momentum space. We assume that the incoming wave is in an initial momentum state p_i and finishes in a final momentum state p_f. We aim to calculate the amplitude $\mathcal{M}$ for the transition between initial and final states. The scattering is elastic, so energy is conserved, $\omega_i = \omega_f$ and $p_i^2 = p_f^2$. For clarity, we adopt the convention that bold-face symbols, e.g. $\boldsymbol{p}_f$, refer to spatial 3-vectors.

Moving to a momentum representation, we may define a scattering amplitude as

$$\mathcal{M} = B(\boldsymbol{p}_f, \boldsymbol{p}_i) + \int \frac{d^3k}{(2\pi)^3} B(\boldsymbol{p}_f, \boldsymbol{k}) \frac{1}{k^2 - \mu^2} B(\boldsymbol{k}, \boldsymbol{p}_i) + \ldots \tag{149}$$

where $B(\boldsymbol{p}_f, \boldsymbol{p}_i)$ is the Fourier transform of the interaction term,

$$B(\boldsymbol{p}_2, \boldsymbol{p}_1) = \int d^3x e^{ip_2\cdot x} \hat{B}(x) e^{-ip_1\cdot x}\,. \tag{150}$$

The differential cross section is related to the amplitude by

$$\frac{d\sigma}{d\Omega} = \frac{1}{4}\frac{|\mathcal{M}|^2}{(2\pi)^2}\,. \tag{151}$$

In the next two section we show how to calculate the first order scalar amplitude in both the Eddington-Finkelstein and Painlevé-Gullstrand coordinate systems.

5.1.2 Amplitude in Eddington-Finkelstein coordinates

Working with AEF coordinates, the difference between the gravitational metric and flat-space metric is

$$g^{\mu\nu} - \eta^{\mu\nu} = \frac{2M}{r}\begin{pmatrix} 1 & -1 \\ -1 & 1 \end{pmatrix}. \tag{152}$$

where the matrix shows the t and r components. The θ and ϕ components are zero. There are four contributions to the interaction corresponding to the four components above, which may be labelled tt, tr, rt, and rr. The easiest to evaluate is the tt term,

$$B_{tt}(\boldsymbol{p}_f, \boldsymbol{p}_i) = -\omega^2 \int d^3x \left(\frac{2M}{r}\right) e^{-i\boldsymbol{q}\cdot\boldsymbol{x}} = \frac{-8\pi\omega^2 M}{|\boldsymbol{q}|^2}, \tag{153}$$

where $\boldsymbol{q} = \boldsymbol{p}_f - \boldsymbol{p}_i$. The rr term may be simplified using integration by parts,

$$\begin{aligned} B_{rr}(\boldsymbol{p}_f, \boldsymbol{p}_i) &= -\int d^3x \frac{\partial}{\partial r}\left(e^{-i\boldsymbol{p}_f\cdot\boldsymbol{x}}\right)\left(\frac{2M}{r}\right)\frac{\partial}{\partial r}\left(e^{i\boldsymbol{p}_i\cdot\boldsymbol{x}}\right) \\ &= 2M\int (i\boldsymbol{p}_f\cdot\boldsymbol{x})(i\boldsymbol{p}_i\cdot\boldsymbol{x})\frac{e^{-i\boldsymbol{q}\cdot\boldsymbol{x}}}{r^3}. \end{aligned} \tag{154}$$

This integral can be solved by employing the sum and difference vectors

$$\boldsymbol{R} = \tfrac{1}{2}\left(\boldsymbol{p}_f + \boldsymbol{p}_i\right), \quad \mathbf{Q} = \tfrac{1}{2}\left(\boldsymbol{p}_f - \boldsymbol{p}_i\right), \tag{155}$$

which allow (154) to be rewritten as

$$B_{rr}(\boldsymbol{p}_f, \boldsymbol{p}_i) = -2M\int d^3x \left[(\boldsymbol{R}\cdot\boldsymbol{x})^2 - (\mathbf{Q}\cdot\boldsymbol{x})^2\right]\frac{e^{-i\boldsymbol{q}\cdot\boldsymbol{x}}}{r^3}. \tag{156}$$

Now let the z-axis be aligned with $\mathbf{Q}$ direction, and the x-axis with the $\boldsymbol{R}$ direction. Then

$$\int d^3x \frac{(\boldsymbol{R}\cdot\boldsymbol{x})^2 e^{-i\boldsymbol{q}\cdot\boldsymbol{x}}}{r^3} = \frac{4\pi|\boldsymbol{R}|^2}{|\boldsymbol{q}|^2} \tag{157}$$

and

$$\int d^3x \frac{(\mathbf{Q}\cdot\boldsymbol{x})^2 e^{-i\boldsymbol{q}\cdot\boldsymbol{x}}}{r^3} = -\frac{4\pi|\mathbf{Q}|^2}{|\boldsymbol{q}|^2}. \tag{158}$$

The total contribution from the rr term is then

$$B_{rr}(\boldsymbol{p}_f, \boldsymbol{p}_i) = -\frac{8\pi M|\boldsymbol{p}|^2}{|\boldsymbol{q}|^2}, \tag{159}$$

since $|\boldsymbol{R}|^2 + |\mathbf{Q}|^2 = |\boldsymbol{p}|^2$.

Finally, we show that the cross terms tr and rt do not contribute at first order. Taking both terms together we have

$$[B_{rt} + B_{tr}](\boldsymbol{p}_f, \boldsymbol{p}_i) = 2i\omega M \int e^{-i\boldsymbol{p}_f\cdot\boldsymbol{x}} \left(\frac{2}{r}\frac{\partial}{\partial r} + \frac{1}{r^2}\right) e^{i\boldsymbol{p}_i\cdot\boldsymbol{x}}. \tag{160}$$

The term with the partial derivative is

$$4i\omega M \int e^{-i\boldsymbol{p}_f\cdot\boldsymbol{x}} \frac{1}{r}\frac{\partial}{\partial r}\left(e^{i\boldsymbol{p}_i\cdot\boldsymbol{x}}\right) = -\frac{4iM\omega\pi^2}{|\boldsymbol{q}|}. \tag{161}$$

The other term has the same magnitude but the opposite sign,

$$2i\omega M \int \frac{e^{-i\boldsymbol{q}\cdot\boldsymbol{x}}}{r^2} = \frac{4i\omega M\pi^2}{|\boldsymbol{q}|}. \tag{162}$$

The net contribution from (160) is therefore zero.

Summing the contributions (153) and (159) yields the first-order amplitude

$$\mathcal{M}_1 = \frac{-8\pi M\left(\omega^2 + |\boldsymbol{p}|^2\right)}{|\boldsymbol{p}_f - \boldsymbol{p}_i|^2}. \tag{163}$$

which may alternatively be expressed as

$$\mathcal{M}_1 = -\frac{2\pi M(1+v^2)}{v^2\sin^2(\theta/2)}, \tag{164}$$

where $v = p/\omega$. Substituting this into (151) gives

$$\boxed{\frac{d\sigma}{d\Omega} = \left(\frac{GM}{c^2}\right)^2 \frac{\left(1+v^2\right)^2}{4v^4\sin^4(\theta/2)}.} \tag{165}$$

5.1.3 Amplitude in Painlevé-Gullstrand coordinates

Below, we show that to first-order, the amplitude in PG coordinates is the same as (164). In this case the difference between the gravitational metric and the flat-space metric is

$$g^{\mu\nu} - \eta^{\mu\nu} = \begin{pmatrix} 0 & -\sqrt{\frac{2M}{r}} \\ -\sqrt{\frac{2M}{r}} & \frac{2M}{r} \end{pmatrix}. \tag{166}$$

The tt term is zero, and the rr term is the same as in the AEF calculation (previous section). The tr terms depend on the square root of M.

Let us consider the sum of the tr and rt terms,

$$\begin{aligned}[B_{tr} + B_{rt}](\boldsymbol{p}_2, \boldsymbol{p}_1) &= 2\sqrt{2M}i\omega \int d^3x e^{-i\boldsymbol{p}_2\cdot\boldsymbol{x}} \frac{1}{r^{1/2}}\left(\frac{\partial}{\partial r} + \frac{3}{4r}\right) e^{i\boldsymbol{p}_i\cdot\boldsymbol{x}} \\ &= 6i\omega\sqrt{M}\pi^{3/2}\frac{{\boldsymbol{p}_2}^2 - {\boldsymbol{p}_1}^2}{|\boldsymbol{p}_2 - \boldsymbol{p}_1|^{7/2}}.\end{aligned} \tag{167}$$

This result is zero when $\boldsymbol{p}_1 = \boldsymbol{p}_i$ and $\boldsymbol{p}_2 = \boldsymbol{p}_f$. In other words, there is no contribution that scales with the half-power $M^{1/2}$. Instead, we must go to next order in the Born series expansion find the term that scales with M. That is, we must evaluate

$$\left(6i\omega\sqrt{M}\pi^{3/2}\right)^2 I, \qquad \text{where} \quad I = \int \frac{d^3k}{(2\pi)^3} \frac{(\boldsymbol{p}^2 - \boldsymbol{k}^2)}{|\boldsymbol{p}_f - \boldsymbol{k}|^{7/2}} \left(\frac{1}{k^2 - \mu^2}\right) \frac{(\boldsymbol{k}^2 - \boldsymbol{p}^2)}{|\boldsymbol{k} - \boldsymbol{p}_i|^{7/2}}. \tag{168}$$

Note that we may immediately cancel the $(k^2 - \mu^2)$ in the denominator with $(\boldsymbol{p}^2 - \boldsymbol{k}^2)$ in the numerator.

Let us calculate the integral I by moving to the centre-of-mass frame. Again, this is achieved with the transformations

$$\begin{aligned} \boldsymbol{k} &\mapsto \boldsymbol{k} + \boldsymbol{R}, \\ \boldsymbol{k}^2 - \boldsymbol{p}^2 &\mapsto \boldsymbol{k}^2 - \mathbf{Q}^2 + 2\boldsymbol{R}\cdot\boldsymbol{k}. \end{aligned} \tag{169}$$

Let us choose the 1-axis to be aligned with $\boldsymbol{R}$ and the 3-axis to be aligned with $\mathbf{Q}$ (note that $\boldsymbol{R}\cdot\mathbf{Q} = 0$) and introduce **spheroidal coordinates**, $\{u, v, \phi\}$:

$$\begin{aligned} k_1 &= |\mathbf{Q}| \sinh u \sin v \cos\phi, \\ k_2 &= |\mathbf{Q}| \sinh u \sin v \sin\phi, \\ k_3 &= |\mathbf{Q}| \cosh u \cos v. \end{aligned} \tag{170}$$

The coordinates lie in the ranges $0 \le u < \infty$, $0 \le v < \pi$, and $0 \le \phi < 2\pi$. The measure of integration is

$$d^3k = |\mathbf{Q}|^3 \sinh u \sin v \left(\sinh^2 u + \sin^2 v\right) du dv d\phi \tag{171}$$

and the important quantities in the integral are

$$\begin{aligned} |\boldsymbol{k} - \mathbf{Q}||\boldsymbol{k} + \mathbf{Q}| &= |\mathbf{Q}|^2(\sinh^2 u + \sin^2 v) \\ \boldsymbol{k}^2 - \mathbf{Q}^2 &= |\mathbf{Q}|^2(\sinh^2 u - \sin^2 v). \end{aligned} \tag{172}$$

Thus the integral becomes

$$I = \frac{1}{(2\pi)^2\mathbf{Q}^2} \int_0^\infty \int_0^\pi \frac{\sinh u \sin v \left(\sinh^2 u - \sin^2 v\right)}{(\sinh^2 u + \sin^2 v)^{5/2}} du dv \tag{173}$$

The integral is straightforward to perform: it is equal to $2/9$. Hence the contribution from the tr and rt terms is

$$-\frac{8\pi M\omega^2}{|\boldsymbol{q}|^2}. \tag{174}$$

Combining (174) and (159) we see that the scattering amplitude at first order in $M\omega$ is identical to that in the Eddington-Finkelstein coordinates, (163).

5.1.4 Spin-half scattering

These techniques can also be applied to the Dirac field. In this case the propagator is defined by

$$\left[i\hat{\gamma}^\mu - m - \hat{B}(x_2)\right] S_G(x_2, x_1) = \delta^4(x_2 - x_1) \tag{175}$$

where $\hat{B}$ depends on the coordinate system. The free-space Feynman propagator is

$$S_(x_2, x_1) = \int \frac{d^4k}{(2\pi)^4} \frac{\hat{\gamma}^\mu k_\mu + \mu}{k^2 - \mu^2} e^{-ik\cdot(x_2 - x_1)} \tag{176}$$

The Dirac scattering amplitude is

$$\mathcal{M} = \bar{u}_s(\boldsymbol{p}_f) V(\boldsymbol{p}_f, \boldsymbol{p}_i) u_r(\boldsymbol{p}_i), \tag{177}$$

where

$$V(\boldsymbol{p}_f, \boldsymbol{p}_i) = B(\boldsymbol{p}_f, \boldsymbol{p}_i) + \int \frac{d^3k}{(2\pi)^3} B(\boldsymbol{p}_f, \boldsymbol{k}) \frac{\not{k} + m}{k^2 - m^2} B(\boldsymbol{k}, \boldsymbol{p}_i) + \cdots \tag{178}$$

and $\bar{u}_s$ and u_r are normalized spinors of spin s and r. Again, $B(\boldsymbol{p}_f, \boldsymbol{p}_i)$ is the spatial Fourier transform of the interaction term,

$$B(\boldsymbol{p}_2, \boldsymbol{p}_1) = \int d^3x e^{-i\boldsymbol{p}_2\cdot\boldsymbol{x}} \hat{B}(\boldsymbol{x}) e^{i\boldsymbol{p}_1\cdot\boldsymbol{x}}. \tag{179}$$

In terms of the amplitude $\mathcal{M}$ the differential cross section is given by

$$\frac{d\sigma}{d\Omega} = \left(\frac{m}{2\pi}\right)^2 |\mathcal{M}|^2 . \tag{180}$$

Exercise: (long!) In either PG or AEF coordinates, show that to first order in M the spinor amplitude is

$$\mathcal{M}_1 = -\frac{4\pi G M}{|\boldsymbol{q}|^2} \overline{u}_s(\boldsymbol{p}_f)(2E\gamma^0 - m) u_r(\boldsymbol{p}_i). \tag{181}$$

This implies a first-order cross section of

$$\boxed{\frac{d\sigma}{d\Omega} = \frac{G^2 M^2}{4v^4 \sin^4(\theta/2)} \left[1 + 2v^2 - 3v^2 \sin^2(\theta/2) + v^4 - v^4 \sin^2(\theta/2)\right]} \tag{182}$$

once the averages over spins are taken.

Perturbative methods may also be applied to the fields of spin 1 and 2. In summary, massless waves ($v = 1$) have the following lowest-order cross sections

$$\lim_{M\omega\to 0} \left(\frac{1}{M^2}\frac{d\sigma}{d\Omega}\right) \approx \begin{cases} \frac{1}{\sin^4(\theta/2)} & s = 0, \quad \text{Scalar wave} \quad [\text{a}] \\ \frac{\cos^2(\theta/2)}{\sin^4(\theta/2)} & s = \frac{1}{2}, \quad \text{Neutrino} \quad [\text{b}] \\ \frac{\cos^4(\theta/2)}{\sin^4(\theta/2)} & s = 1, \quad \text{Photon} \quad [\text{c}] \\ \frac{\cos^8(\theta/2) + \sin^8(\theta/2)}{\sin^4(\theta/2)} & s = 2, \quad \text{Grav. wave} \quad [\text{d}]. \end{cases} \tag{183}$$

It is worth noting that the gravitational result is somewhat anomalous, in that it doesn't follow the same general rule $\left[d\sigma/d\Omega = M^2 \cos^{4s}(\theta/2)/\sin^4(\theta/2)\right]$ as the other fields.

5.2 Partial Wave Analysis

Perturbative approximations are only really appropriate when the coupling is small, $M\omega \ll 1$. Beyond this regime, an alternative method is required. In this section, we treat the scattering of scalar waves through a partial-wave expansion.

A plane wave can be decomposed into a sum of angular modes as

$$\Phi_{\text{plane}} = e^{ipz} \sim \frac{1}{2ipr}\sum_{l=0}^{\infty}(2l+1)P_l(\cos\theta)\left[e^{ipr} + (-1)^{l+1}e^{-ipr}\right]. \tag{184}$$

Here, $p = \sqrt{\omega^2 - \mu^2}$. On a black hole space-time, we are unable to construct a plane wave from solutions of the free wave equation, because the radial component goes as $e^{\pm ipr_*}$ at infinity. This introduces a logarithmic phase shift, so that the wavefronts are distorted even at large r. A similar caveat is true in the case of EM scattering from the Coulomb potential; it is a simple consequence of the $1/r$ tail of the potential. A distorted wave $\Phi^{\text{dist.}}_{\text{plane}}$ is obtained by replacing $r \to$ with r_* in the exponents of (185), i.e.

$$\Phi^{\text{dist.}}_{\text{plane}} = \frac{1}{2ipr}\sum_{l=0}^{\infty}(2l+1)P_l(\cos\theta)\left[e^{ipr_*} + (-1)^{l+1}e^{-ipr_*}\right]. \tag{185}$$

It is the 'nearest approximation' to the plane wave in a black hole space-time.

Let us construct a partial wave solution

$$\Phi \sim \Phi^{\text{dist.}}_{\text{plane}} + \frac{f(\theta)}{r}e^{ipr_*} = \frac{1}{r}\sum_{l=0}^{\infty} a_l P_l(\cos\theta)\phi_l^{(\text{in})}(r_*). \tag{186}$$

Here, $\phi_l^{(\text{in})}(r_*)$ are the solutions defined by boundary conditions (114). The series coefficients a_l may be found by matching the ingoing e^{-ipr_*} part of (186) to the ingoing part of the distorted plane wave. Hence

$$f(\theta) = \frac{1}{2i\omega}\sum_{l=0}^{\infty}(2l+1)\left(e^{2i\delta_l} - 1\right)P_l(\cos\theta). \tag{187}$$

where

$$e^{2i\delta_l} = (-1)^{l+1}\frac{A_{\text{out}}}{A_{\text{in}}} \tag{188}$$

[***Exercise***: Show this].

The differential scattering cross section is simply

$$\frac{d\sigma}{d\Omega} = |f(\theta)|^2 \tag{189}$$

where $d\Omega$ is an element of solid angle.

In addition to scattering flux, the black hole may also absorb incident radiation. The **transmission factor** $\mathbb{T}_l$ for each mode is

$$\mathbb{T}_l = 1 - \left|e^{2i\delta_l}\right| \tag{190}$$

Transmission corresponds to the imaginary part of the phase shifts δ_l. The total absorption cross section is found from a sum over modes:

$$\sigma_{\rm abs} = \frac{\pi}{\omega^2}\sum_{l=0}^{\infty}(2l+1)\mathbb{T}_l \tag{191}$$

In a moment, we show absorption cross sections for various couplings $M\omega$.

[***Exercise***: Derive expression (191) for the absorption cross section.

- Start with

$$\lim_{r\to\infty}\Phi \sim \frac{1}{2ipr}\sum_{l=0}^{\infty}(2l+1)P_l(\cos\theta)\left((-1)^{l+1}e^{-ipr_*}+e^{2i\delta_l}e^{ipr_*}\right). \tag{192}$$

- Deduce an expression for the ingoing flux passing through a sphere of radius r in the limit $r\to\infty$. (Use the expression for the probability current J_r and integrate over solid angle. The apply the identity

$$\int_0^{\pi}\sin\theta P_l(\cos\theta)P_{l'}(\cos\theta)d\theta = \frac{2\delta_{ll'}}{2l+1}. \tag{193}$$

  Remove inconvenient cross terms by taking an average over time.)

- Divide the total flux through the sphere by the flux of the incoming wave to get result (191).

The phase shifts and transmission factors may be approximated analytically, or computed numerically. Here we will consider the low-coupling regime, and then tackle the problem numerically.

5.2.1 The comparison Newtonian problem

For the scalar wave, a low-coupling approximation may be derived by considering the small-$M\omega$ limit of the scalar wave equation. First, we make the substitution $u = (1-2M/r)^{-1/2}y$ in equation (41). Then the radial equation in the Schwarzschild coordinate system becomes

$$\left[\left(1-\frac{2M}{r}\right)^2\frac{d^2}{dr^2}+\left(\omega^2+\frac{M^2}{r^4}\right)-\left(1-\frac{2M}{r}\right)\left(\frac{l(l+1)}{r^2}+\mu^2\right)\right]y = 0. \tag{194}$$

Let us now expand this equation in the large-r limit and only keep terms up to r^{-3}. We find

$$\frac{d^2y}{dr^2}+\left[(\omega^2-\mu^2)+\frac{2M(2\omega^2-\mu^2)}{r}+\frac{4M^2(3\omega^2-\mu^2)-l(l+1)}{r^2}+\mathcal{O}\left(\frac{1}{r^3}\right)\right]y = 0 \tag{195}$$

In the limit $l(l+1)\gg(M\omega)^2$ and $l(l+1)\gg(M\mu)^2$ the angular momentum barrier term in the potential, which goes as $1/r^2$, dominates over all higher-order terms. Neglecting terms of r^{-3} and higher, we see that equation (195) is the same as the radial equation for non-relativistic Coulomb scattering, if $\beta_C = Z\alpha\mu/p$ is replaced by

$$\beta_G = \frac{M(2\omega^2-\mu^2)}{p}. \tag{196}$$

The "Newtonian" phase shifts are therefore the same as for the non-relativistic Coulomb scattering problem

$$e^{2i\delta_l^N} = \frac{\Gamma(l+1-i\beta)}{\Gamma(l+1+i\beta)}. \tag{197}$$

It is well known that the problem of non-relativistic Coulomb scattering can be solved exactly in parabolic coordinates. Hence the "Newtonian" phase shift series may be summed using the Coulomb result to

$$f_N(\theta) \equiv \frac{1}{2ip}\sum_{l=0}\frac{\Gamma(l+1-i\beta)}{\Gamma(l+1+i\beta)}(2l+1)P_l(\cos\theta) = \frac{\beta}{2p}\frac{\Gamma(1-i\beta)}{\Gamma(1+i\beta)}\left[\sin(\theta/2)\right]^{-2+2i\beta}. \tag{198}$$

It is more difficult to sum the series *directly*, because it is poorly convergent. This is related to the fact that an infinite number of Legendre polynomials are required to describe the divergence at $\theta = 0$.

The Newtonian scattering cross section is simply $|f_N|^2$, that is,

$$\frac{d\sigma}{d\Omega} = \frac{\beta^2}{4p^2\sin^4(\theta/2)} = \frac{M^2(1+v^2)^2}{4v^4\sin^4(\theta/2)}. \tag{199}$$

It is interesting to note that this is exactly the same cross section as was derived via perturbation theory at first order (165). This result is equivalent to the Rutherford scattering cross section for electromagnetic scattering. Note that the cross section diverges as θ^{-4} in the forward direction. It is the $1/r$ term in the potential that is responsible for this divergence, and an infinite number of partial waves contribute to it.

5.2.2 Partial wave amplitudes

To calculate the scattering amplitude we need to determine the phase shifts. These may be computed using direct numerical integration of the radial wave equation. Figure 13 shows numerical phase shifts as a function of angular momentum, l, for the scalar wave at $M\omega = 2$. The real part of $e^{2i\delta_l}$ is compared with the real part of $e^{2i\delta_l^{(N)}}$ from the "comparison Newtonian problem" of section 5.2.1. The Newtonian phase is matched to the numerical phase at $l = 80$. Note that waves of low angular momentum are partially absorbed by the black hole, as $|e^{2i\delta_l}| < 1$.

Due to finite computing power, the partial wave series must be truncated at a certain value of $l = l_{\max}$. With modern computing power, it is easy to compute phase shifts up to $l \sim 80$. This may seem impressive but the partial wave series are poorly convergent. An infinite number of partial waves are required to correctly describe the divergence in the amplitude at $\theta = 0$.

For the scalar wave, it is possible to get round the convergence problem by using results from the "comparison Newtonian problem". The amplitude can be split into two parts, $f = f_{\text{diff}} + f_{\text{Newt}}$. The amplitude f_{diff} is computed from the difference between the numerical phase shifts and the Newtonian phase shifts. The Newtonian amplitude f_{Newt} is known analytically. The overall phase of the scattered wave is fixed so that the numerical and Newtonian phase shifts match at $l = l_{\max}$. Any remaining difference above $l_{\max}$ is neglected. This method works very well for the scalar wave, but fails for waves of higher spin. Here we outline an alternative method.

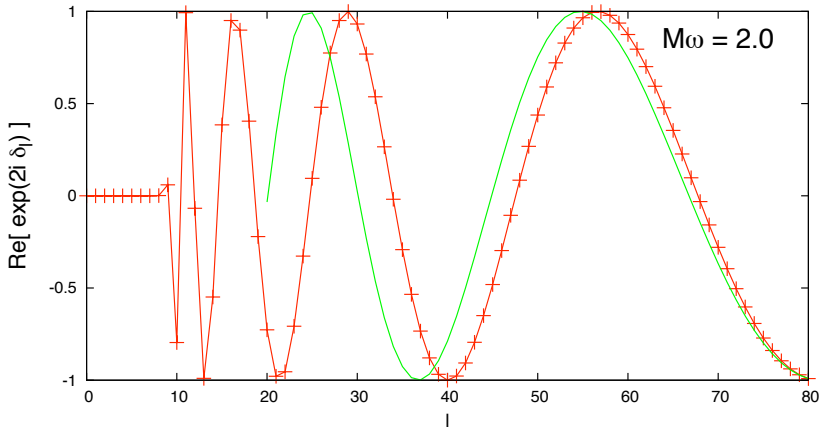

Figure 13: *Scalar wave phase shifts at* $M\omega = 2$. The real part of $S_l = e^{2i\delta_l}$ [red] is compared with the "Newtonian" phase shifts [green] of equation (197). The results for two speeds $v = 1.0$ (top) and $v = 0.2$ (bottom) are shown. .

Given a Legendre polynomial series

$$f(\theta) = \sum_{l=0} a_l^{(0)} P_l(\cos\theta) \tag{200}$$

that is divergent at $\theta = 0$, one may define the mth reduced series,

$$(1 - \cos\theta)^m f(\theta) = \sum_{l=0} a_l^{(m)} P_l(\cos\theta). \tag{201}$$

The reduced series is obviously less divergent at $\theta = 0$, so one may hope that the reduced series converges more quickly. Using the properties of the Legendre polynomials, it is straightforward to show that the new coefficients $a_l^{(i+1)}$ are related to the old coefficients $a_l^{(i)}$ by the iterative formula

$$a_l^{(i+1)} = a_l^{(i)} - \frac{l+1}{2l+3} a_{l+1}^{(i)} - \frac{l}{2l-1} a_{l-1}^{(i)}. \tag{202}$$

I have found this to be an excellent method for summing the series numerically, and two or three iterations are sufficient.

[***Exercise***: Use the Legendre polynomial recurrence relation

$$lP_l(x) = x(2l-1)P_{l-1} - (l+m-1)P_{l-2} \tag{203}$$

to prove result (202).]

Figures 14 and 15 show numerically-determined scattering cross sections for the massless scalar and spinor waves. There are oscillations at intermediate angles suggestive of diffractive effects. The magnitude of the oscillations, and their angular frequency, increases with black hole mass. The massless scalar wave has a peak on-axis in the backward direction (called a *glory*), whereas the massless spinor wave tends to zero here.

The origin of the oscillations in the cross section can be understood from geometric arguments. Consider a pair of geodesics scattered by a Schw. hole, passing around the hole in

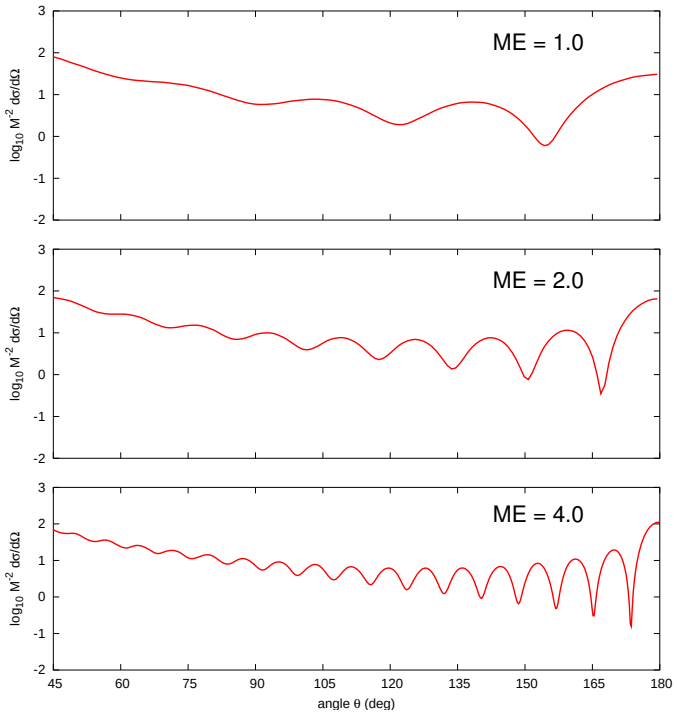

Figure 14: *Scalar scattering cross sections.* Shows the massless scalar wave cross section for various couplings $ME \equiv GM\omega/c^3$. Note the logarithmic scale on the y-axis.

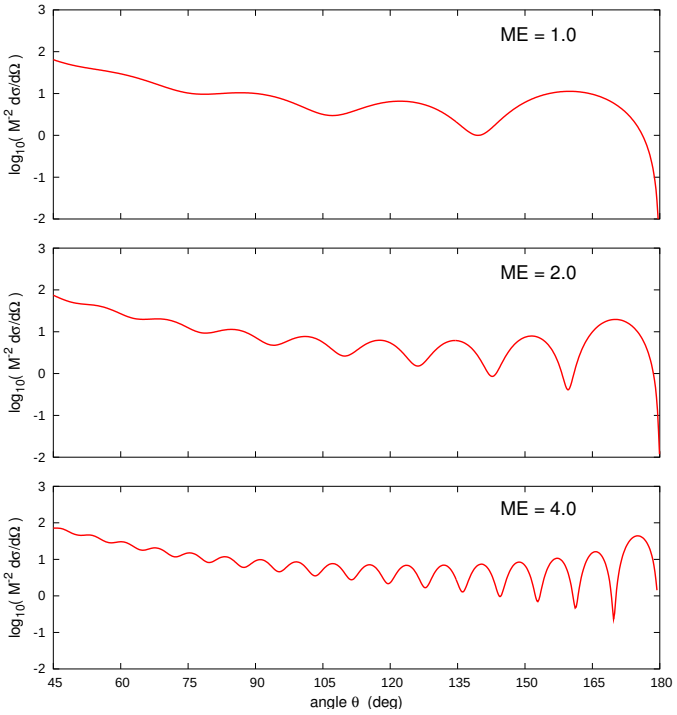

Figure 15: *Spinor scattering cross sections.* Shows the massless spin-half cross section for various couplings $ME \equiv GM\omega/c^3$.

opposite senses (i.e. clockwise and counter-clockwise). If one geodesic is scattered through an angle θ and the other is scattered through an angle $2\pi - \theta$ they will emerge in the same direction. There will be a path difference between the two rays which depends on the angle of scattering. If the path difference is an integer number of wavelengths then constructive interference arises; if it is a half-integer multiple of λ then destructive interference results.

Black hole wave scattering also produces a diffraction effect familiar from optical phenomena: a *glory*. A glory is a bright spot or halo that appears on-axis in the backward direction from the scatterer.

Ford and Wheeler [7] derived a semi-classical approximation of the glory scattering cross section for scalar ($s = 0$) waves. The approximation may be extended to arbitrary spins [20] using path integral methods. For massless waves, the backward glory cross section is approximated by

$$\left.\frac{d\sigma}{d\Omega}\right|_{\text{glory}} \approx 2\pi E {b_g}^2 \left|\frac{db}{d\theta}\right|_{\theta=\pi} {J_{2s}}^2(Eb_g \sin\theta), \tag{204}$$

where s is the spin of the particle, J_{2s} is a Bessel function, and b_g is the impact parameter at which backward scattering occurs, $\theta = \pi$.

To find b_g one must integrate the orbit equation (**??**). The exact solutions $u(\phi)$ describing the scattering trajectories may be expressed in terms of elliptic functions. By using asymptotic results for elliptic functions it is possible to show that for geodesics passing close to the unstable orbit,

$$b - b_c \approx 216 \times b_c \times \left(\frac{\sqrt{3}-1}{\sqrt{3}+1}\right)^2 e^{-\pi} e^{-\theta} \approx 3.48 M e^{-\theta} \tag{205}$$

where $b_c = 3\sqrt{3}M$.

Hence we have $b_g \approx 5.3465M$, and $|db/d\sigma| = 0.1504M$, so

$$M^{-2} \left.\frac{d\sigma}{d\Omega}\right|_{\text{glory}} \approx 2\pi EM \times 4.30 \times {J_{2s}}^2(5.3465 EM \sin\theta). \tag{206}$$

For the scalar wave, the intensity has a peak in the backwards direction, whereas for the spinor wave the intensity is zero on-axis.

5.2.3 Absorption

In addition to scattering the incident wave, the black hole will absorb a proportion of the incident flux. The absorption cross section (191) is found a sum over the transmission factors (190). Transmission factors for the first few modes are shown in Fig. 16. They are plotted as a function of the dimensionless coupling $M\omega \equiv GM\omega/c^3$.

Figure 17 shows the absorption cross section as a function of coupling $M\omega$. The oscillatory pattern is due to the contribution of successive modes. At low couplings (i.e. $\lambda \gg r_s$), the cross section tends to $\sigma_a = 16\pi M^2$. At high couplings ($\lambda \ll r_s$) the cross sections tends to the geometric optics value of $\sigma_a = \pi(b_c)^2 = 27\pi M^2$.

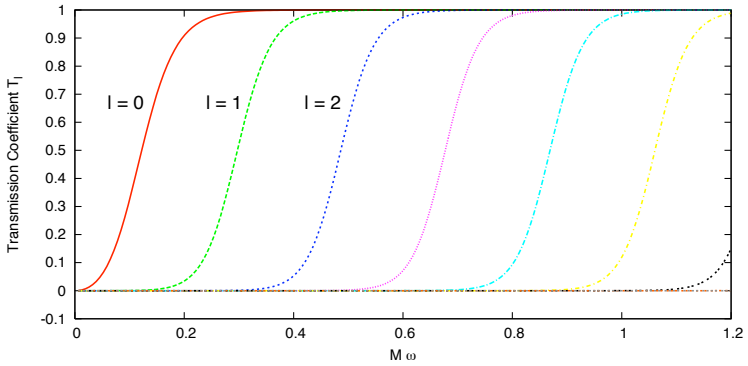

Figure 16: *Modal transmission factors for the massless scalar wave absorbed by a Schwarzschild black hole.*

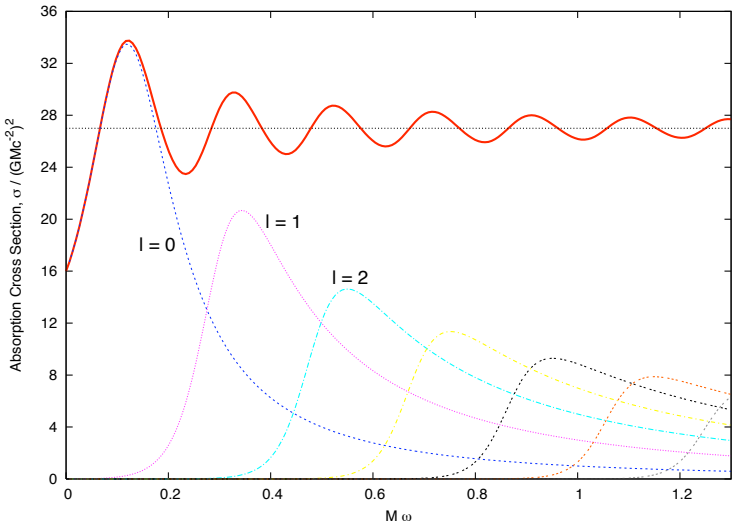

Figure 17: *Absorption cross section for a massless scalar wave impinging upon a Schwarzschild black hole.* The thick line shows the total cross section as a function of coupling $M\omega$. The thin lines show the contributions from the partial modes. The dotted line at $y = 27$ shows the high-frequency limit, $\sigma_{\rm abs} = \pi b_c^2$.

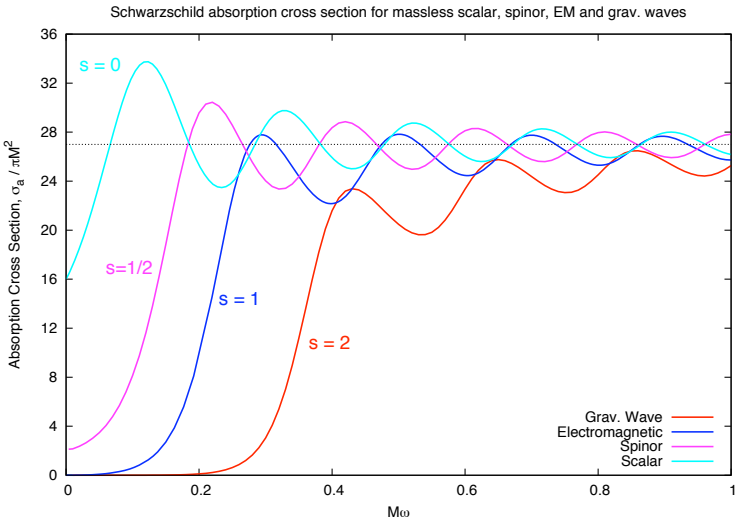

Figure 18: *Absorption cross section for massless scalar, neutrino, electromagnetic and gravitational waves impinging upon a Schwarzschild black hole.* The electromagnetic cross section is reproduced from LCB Crispino, ES Oliveira, A Higuchi and GEA Matsas, *Phys. Rev. D* **75**, 104012 (2007) with kind permission from the authors.

It turns out that the absorption cross section in the long-wavelength limit depends on the spin of the wave under consideration.

$$\lim_{M\omega\to 0}\sigma_a = \begin{cases} 16\pi M^2 & s=0 \\ 2\pi M^2 & s=1/2 \\ 0 & s=1 \text{ or } 2 \end{cases} \tag{207}$$

In other words, electromagnetic and gravitational waves with very long wavelengths ($\lambda \gg r_S$) are not absorbed. In the short-wavelength ($\lambda \ll r_s$) semi-classical limit, the spin is not so significant, and all cross sections tend to the geometric optics value. This behaviour is clearly shown in Fig. 18.

6 Further Topics*

6.1 The Dirac Equation

In this section we show how to formulate the Dirac equation on the Schwarzschild space-time. We start by reviewing tetrad theory, and show how tetrads are used to construct a covariant derivative operator for the spin-half field. Next, we consider the Dirac equation in a general coordinate system, and show how to separate out the angular part to leave two coupled first-order equations for the radial functions. We conclude with a discussion of the probability current, and the behaviour of solutions at the horizon and at infinity.

We expect the Dirac equation on a gravitational background to take a similar form to the Minkowski Dirac Equation (65), that is

$$i\hat{\gamma}^\mu \hat{D}_\mu(x^\nu)\psi = \mu\psi \tag{208}$$

where $\hat{D} = \hat{\gamma}^\mu \hat{D}_\mu(x^\nu)$ is a 4×4 derivative operator that is a function of the coordinates. In the next section we show how to construct a derivative operator that behaves correctly under coordinate transformations, and local rotations and boosts.

The precise form of the Dirac equation depends not just on our choice of coordinate system, but also on a choice of local *tetrad field*. A 'tetrad field' is a basis of vectors that may vary from point to point in the space-time. Unlike the scalar field, the Dirac field will 'feel' rotational effects (such as frame-dragging) that act through the tetrad field. In other words, we must set up the equations to allow for a coupling between the spin of the field and the geometry of space-time.

Ultimately, any physical predictions of the theory must be independent of the choice of coordinates, and also independent of the choice of tetrad field. Together, we call the coordinate system and the tetrad the 'gauge' degrees of freedom. Our ultimate aim is to extract observables that are 'gauge-invariant'. In general, the higher the spin of the field, the greater the number of degrees of gauge freedom.

6.1.1 Tetrads and the spin-connection

A non-coordinate basis $\hat{\mathbf{e}}^a$ and $\hat{\mathbf{e}}_a$ may be defined in terms of the coordinate basis dx^μ, ∂_μ by introducing a *tetrad* (or *vierbien*) field $e_a{}^\mu$ and its inverse $e^a{}_\mu$, so that

$$\hat{\mathbf{e}}^a = e^a{}_\mu dx^\mu, \qquad \hat{\mathbf{e}}_a = e_a{}^\mu \partial_\mu. \tag{209}$$

Here, roman letters $(a, b, c, \ldots)$ will be used for the non-coordinate basis, and greek letters $(\mu, \nu, \lambda, \ldots)$ for the coordinate basis. The non-coordinate basis may be assumed to be orthonormal, with Lorentzian inner products $\hat{\mathbf{e}}_a \cdot \hat{\mathbf{e}}_b = \eta_{ab} = \mathrm{diag}[1, -1, -1, -1]$. Alternatively the basis vectors may chosen to be null; this is the starting point for the Newman-Penrose formalism.

With an orthonormal basis, the metric is defined by

$$g_{\mu\nu} = e^a{}_\mu e^b{}_\nu \eta_{ab}, \qquad \eta_{ab} = e_a{}^\mu e_b{}^\nu g_{\mu\nu}. \tag{210}$$

Tensors can be expressed in terms of non-coordinate components,

$$X = X^a{}_b \hat{\mathbf{e}}_a \otimes \hat{\mathbf{e}}^b = X^\mu{}_\nu \partial_\mu \otimes dx^\nu \,, \tag{211}$$

and the coordinate and non-coordinate components are related by

$$X^a{}_b = e^a{}_\mu e_b{}^\nu X^\mu{}_\nu \,. \tag{212}$$

The *spin-connection* $\omega_\mu{}^a{}_b$ is defined by

$$\nabla_\mu X^a = \partial_\mu X^a + \omega_\mu{}^a{}_b X^b \,, \tag{213}$$

where ∇_μ denotes the covariant derivative with respect to coordinate x^μ. In other words, the spin-connection plays the role of the affine connection when we take a covariant derivative of a quantity resolved on to the orthonormal basis.

The spin-connection is related to the affine connection $\Gamma^{\mu}{}_{\nu\lambda}$ by

$$\omega_{\mu}{}^{a}{}_{b} = e^{a}{}_{\nu} e_{b}{}^{\lambda} \Gamma^{\nu}{}_{\mu\lambda} - e_{b}{}^{\lambda} \partial_{\mu} e^{a}{}_{\lambda} \,. \tag{214}$$

where

$$\Gamma^{\mu}\sigma\lambda = \tfrac{1}{2} g^{\mu\nu} \left(\partial_{\lambda} g_{\nu\sigma} + \partial_{\sigma} g_{\lambda\nu} - \partial_{\nu} g_{\sigma\lambda} \right) \tag{215}$$

The spin-connection can also be determined without first calculating the affine connection, by use of the Ricci rotation coefficients γ_{abc}. These are related to the spin-connection by

$$\gamma_{abc} = -e_{c}{}^{\mu} \omega_{\mu ab} \tag{216}$$

and can be calculated through the pre-rotation coefficients λ_{abc}:

$$\gamma_{abc} = \frac{1}{2} \left(\lambda_{abc} + \lambda_{cab} - \lambda_{bca} \right) \,, \tag{217}$$

where

$$\lambda_{abc} = \left(e_{b\mu,\nu} - e_{b\nu,\mu} \right) e_{a}{}^{\mu} e_{c}{}^{\nu} \,. \tag{218}$$

The pre-rotation coefficients λ_{abc} are antisymmetric under the interchange of first and last indices, and the Ricci rotation coefficients γ_{abc} are antisymmetric under the interchange of the first pair of indices. For more details on this approach, see for example Chandrasekhar's book [3].

6.1.2 Derivative operator for the Dirac field

The tensor equations of GR are covariant: they do not change in form under general coordinate transformations (GCTs). Equations written in terms of a tetrad basis must transform correctly under GCTs, and they must also transform correctly under Local Lorentz Transformations (LLTs) of the non-coordinate frame. In this section, we briefly demonstrate how these requirements constrain the derivative operator for the Dirac wavefunction. For more detail on this approach, see for example Nakahara [15]. These ideas are succinctly expressed in the Gauge Theory of Gravity (GTG) formulated by Lasenby, Doran and Gull [10].

Under an infinitessimal Local Lorentz Transformation $\Lambda^{a}{}_{b} = \delta^{a}_{b} + \epsilon^{a}{}_{b}$, the Dirac wavefunction ψ transforms as

$$\psi \rightarrow \psi' = \rho(\Lambda)\psi \qquad \text{where} \quad \rho(\Lambda) = 1 + \frac{i}{2} \epsilon_{ab} \hat{\Sigma}^{ab} \tag{219}$$

and

$$\hat{\Sigma}^{ab} = \frac{i}{4} \left[\hat{\gamma}^{a}, \hat{\gamma}^{b} \right] . \tag{220}$$

The derivative of the wavefunction must transform as a vector under a LLT. That is,

$$\hat{D}_{a}\psi \rightarrow \hat{D}'_{a}\psi' = \rho(\Lambda) \Lambda_{a}{}^{b} \hat{D}_{b}\psi. \tag{221}$$

To be covariant under a GCT the derivative must include the tetrad field. To transform correctly under LLTs, $\hat{D}_{a}$ must also include an extra term, so that

$$\hat{D}_{a} = e_{a}{}^{\mu} \left(\partial_{\mu} + \Omega_{\mu} \right) . \tag{222}$$

Under LLTs, the transformation property (221) requires that

$$\Omega_\mu \to \Omega'_\mu = \rho\Omega_\mu\rho^{-1} - (\partial_\mu\rho)\rho^{-1}. \tag{223}$$

It turns out that the spin-connection $\omega_{\mu ab}$ provides the required transformation properties (see Nakahara [15]) and that

$$\Omega_\mu = \frac{i}{2}\omega_{\mu ab}\hat{\Sigma}^{ab}. \tag{224}$$

The Dirac equation on a general background can then be written as

$$i\hat{\gamma}^a e_a{}^\mu \left(\partial_\mu + \frac{i}{2}\omega_{\mu bc}\hat{\Sigma}^{bc}\right)\psi = \mu\psi. \tag{225}$$

The Ricci rotation coefficients γ_{abc}, and thus the spin-connection, are easily calculated with the aid of a symbolic algebra package, such as GRTensor [14] and Maple.

6.1.3 The Dirac equation on a Schwarzschild background

In this section we formulate the Dirac equation on the Schwarzschild background, following the approach of Lasenby *et al.* [11]. We start with the most general possible form that satisfies the constraints of spherical symmetry, and use this form to guarantee that various expressions are gauge invariant.

Let $\{\gamma_0, \gamma_1, \gamma_2, \gamma_3\}$ denote the standard gamma matrices in the Dirac–Pauli representation, defined in equation (67). Next, introduce polar coordinates $\{r, \theta, \phi\}$. From these we may define the unit polar matrices by

$$\begin{aligned}
\gamma_r &= \sin\theta(\cos\phi\,\gamma_1 + \sin\phi\,\gamma_2) + \cos\theta\,\gamma_3\,, \\
\gamma_\theta &= \cos\theta(\cos\phi\,\gamma_1 + \sin\phi\,\gamma_2) - \sin\theta\,\gamma_3\,, \\
\gamma_\phi &= -\sin\phi\,\gamma_1 + \cos\phi\,\gamma_2.
\end{aligned} \tag{226}$$

In terms of these we define the four matrices representing the non-coordinate basis,

$$\begin{aligned}
g^t &= a_1\gamma_0 - a_2\gamma_r, & g^\theta &= -\frac{1}{r}\gamma_\theta, \\
g^r &= -b_1\gamma_r + b_2\gamma_0, & g^\phi &= -\frac{1}{r\sin\theta}\gamma_\phi,
\end{aligned} \tag{227}$$

where (a_1, a_2, b_1, b_2) are scalar functions of r satisfying

$$\begin{aligned}
a_1 b_1 - a_2 b_2 &= 1, \\
(b_1)^2 - (b_2)^2 &= 1 - 2M/r.
\end{aligned} \tag{228}$$

The reciprocal set of matrices are therefore

$$\begin{aligned}
g_t &= b_1\gamma_0 - b_2\gamma_r & g_\theta &= r\gamma_\theta \\
g_r &= a_1\gamma_r - a_2\gamma_0 & g_\phi &= r\sin\theta\gamma_\phi.
\end{aligned} \tag{229}$$

These matrices satisfy

$$\begin{aligned}\{g^\mu, g^\nu\} &= 2g^{\mu\nu} I \\ \{g_\mu, g_\nu\} &= 2g_{\mu\nu} I \\ \{g^\mu, g_\nu\} &= 2\delta^\mu_\nu I\end{aligned} \tag{230}$$

where μ, ν run over the set (t, r, θ, ϕ), I is the identity matrix, and $\{g^\mu, g^\nu\} = g^\mu g^\nu + g^\nu g^\mu$. The line element defined by this metric is

$$g_{\mu\nu} dx^\mu dx^\nu = \big(1 - 2M/r\big) dt^2 + 2\big(a_1 b_2 - a_2 b_1\big) dt\, dr - \big((a_1)^2 - (a_2)^2\big) dr^2 - r^2 d\Omega^2. \tag{231}$$

This line element is the most general form one can adopt for the Schwarzschild solution. There is only one degree of freedom in equation (231), since the terms are related by

$$(1 - 2M/r)\big((a_1)^2 - (a_2)^2\big) + (a_1 b_2 - a_2 b_1)^2 = 1. \tag{232}$$

As discussed for the KG equation in section 3.1.3, this degree of freedom corresponds to the fact that the time coordinate is only defined up to an arbitrary radially-dependent term. As before, let us examine the consequences of a transformation of the time coordinate,

$$t \to t + \alpha(r). \tag{233}$$

The new line element will be independent of the new time coordinate. Rather than think in terms of changing the time coordinate, it is simpler for our purposes to always label the time coordinate as t and instead redefine a_1 and a_2. These then transform as

$$\begin{aligned} a_1 &\mapsto \tilde{a}_1 = a_1 - b_2 \alpha' \\ a_2 &\mapsto \tilde{a}_2 = a_2 - b_1 \alpha', \end{aligned} \tag{234}$$

with b_1 and b_2 unchanged. Throughout, dashes denote derivatives with respect to r. It is straightforward to confirm that the new set $(\tilde{a}_1, \tilde{a}_2, b_1, b_2)$ still satisfy the constraints (228).

The four variables a_1, a_2, b_1 and b_2 are subject to two constraint equations, so must contain two arbitrary degrees of freedom. The first arises from the freedom in the time coordinate as described in equation (234). The second lies in the freedom to perform a radially-dependent boost (a LLT), which transforms the variables according to

$$\begin{pmatrix} a_1 & b_1 \\ a_2 & b_2 \end{pmatrix} \mapsto \begin{pmatrix} \cosh\beta & \sinh\beta \\ \sinh\beta & \cosh\beta \end{pmatrix} \begin{pmatrix} a_1 & b_1 \\ a_2 & b_2 \end{pmatrix}, \tag{235}$$

where β is an arbitrary, non-singular function of r. This boost does not alter the line element of equation (231). Outside the horizon we have $|b_1| > |b_2|$, and in the asymptotically flat region b_1 can be brought to $+1$ by a suitable boost. It follows that we must have

$$b_1 > 0 \quad \forall r \geq 2M. \tag{236}$$

At the horizon we therefore have b_1 positive, and $b_2 = \pm b_1$. For black holes (as opposed to white holes) the negative sign is the correct one, as this choice guarantees that particles fall across the

horizon in a finite coordinate time. This sign is also uniquely picked out by models in which the black hole is formed by a collapse process. We can therefore write

$$b_2 = -b_1 \quad \text{at } r = 2M. \tag{237}$$

Combining this with the identity $a_1 b_1 - a_2 b_2 = 1$ we find that, at the horizon, we must have

$$a_1 b_2 - a_2 b_1 = -1 \quad \text{at } r = 2M. \tag{238}$$

The diagonal form of the Schwarzschild metric sets $a_1 b_2 - a_2 b_1 = 0$, so does not satisfy this criterion. But for this case the time coordinate t is only defined outside the horizon, and the horizon itself is not dealt with correctly.

We now have a general parameterisation of the Schwarzschild solution in an arbitrary gauge, which we can substitute into our expression for the Dirac equation (225). The components of the spin connection may be found through the Ricci rotation coefficients. These turn out to give

$$g^\mu \frac{i}{2} \omega_\mu{}^{ab} \Sigma_{ab} = \tfrac{1}{2} \left(b_2' + \frac{2b_2}{r} \right) \gamma_0 - \tfrac{1}{2} \left(b_1' + \frac{2(b_1 - 1)}{r} \right) \gamma_r \tag{239}$$

which may be substituted into (225).

Table 1: Tetrad functions for three coordinate systems.

Schwarzschild :	$a_1 = (1 - 2M/r)^{-1/2}$	$b_1 = (1 - 2M/r)^{1/2}$
	$a_2 = 0$	$b_2 = 0$
Advanced EF :	$a_1 = 1 + M/r$	$b_1 = 1 - M/r$
	$a_2 = M/r$	$b_2 = -M/r$
Painlevé-Gullstrand:	$a_1 = 1$	$b_1 = 1$
	$a_2 = 0$	$b_2 = -\sqrt{2M/r}$

References

[1] Andersson, N., and Jensen, B. P. Scattering by black holes. *gr-qc/0011025* (2001).

[2] C. .W. Misner, K. S. T., and Wheeler, J. A. *Gravitation.* W.H. Freeman, New York, 1973.

[3] Chandrasekhar, S. *The Mathematical Theory of Black Holes.* Oxford University Press, 1983.

[4] d'Inverno, R. *Introducing Einstein's Relativity.* Oxford University Press, Oxford, 1992.

[5] Dolan, S. R., Doran, C. J. L., and Lasenby, A. N. Fermion scattering by a Schwarzschild black hole. *Phys. Rev. D* **74** (2006), 064005.

[6] Doran, C. J. L., and Lasenby, A. N. Perturbation theory calculation of the black hole elastic scattering cross section. *Phys. Rev. D* **66** (2002), 024006.

[7] Ford, K. W., and Wheeler, J. A. Semiclassical description of scattering. *Ann. Phys. (NY)* **7** (1959), 259.

[8] Frolov, V. P., and Novikov, I. D. *Black Hole Physics: Basic Concepts and New Developments.* Kluwer Academic Publishers, Dordrecht, 1998.

[9] Greiner, W. *Relativistic Quantum Mechanics.* Springer-Verlag, 1990.

[10] Lasenby, A. N., Doran, C. J. L., and Gull, S. F. Gravity, gauge theories and geometric algebra. *Phil. Trans. R. Soc. Lond. A* **356** (1998), 487–582.

[11] Lasenby, A. N., Doran, C. J. L., Pritchard, J., Caceres, A., and Dolan, S. R. Bound states and decay times of fermions in a Schwarzschild black hole background. *Phys. Rev. D* **72** (2005), 105014.

[12] Leaver, E. W. An analytic representation for the quasi-normal modes of Kerr black holes. *Proc. R. Soc. London A* **402** (1985), 285.

[13] Leaver, E. W. Spectral decomposition of the perturbation response of the Schwarzschild geometry. *Phys. Rev. D* **34** (1986), 384.

[14] Musgrave, P., Pollney, D., and Lake, K. GRTensorII: A package for general relativity. *Fields Institute Communications* **15** (1996), 313–318.

[15] Nakahara, M. *Geometry, Topology and Physics.* Adam Hilger, Bristol, 1990.

[16] Poisson, E. *A Relativist's Toolkit: The Mathematics of Black Hole Mechanics.* Cambridge University Press, Cambridge, 2004.

[17] Schutz, B. F., and Will, C. M. Black hole normal modes - A semianalytic approach. *Astrophysical Journal Letters* **291** (1985), L33–L36.

[18] Schwarzschild, K. Uber das Gravitationsfeld eines Massenpunktes nach der Einsteinschen Theorie. *Sitzber. Deut. Akad. Wiss. Berlin* (1916), 189–196.

[19] Vishveshwara, C. V. Scattering of gravitational radiation by a Schwarzschild black hole. *Nature* **227** (1970), 936–938.

[20] Zhang, T.-R., and DeWitt-Morette, C. WKB cross section for polarized glories of massless waves in curved space-times. *Phys. Rev. Lett.* **52** (1984), 2313–2316.